이학박사 학위논문

Cosmology of Light Scalar Dark Matters

가벼운 스칼라 암흑물질의 우주론

2021 년 2 월

서울대학교 대학원

물리천문학부 물리학전공

김 현 태

Cosmology of Light Scalar Dark Matters

가벼운 스칼라 암흑물질의 우주론

지도교수 김 형 도

이 논문을 이학박사 학위논문으로 제출함

2021 년 1 월

서울대학교 대학원

물리천문학부 물리학 전공

김 현 태

김현태의 이학박사 학위논문을 인준함

2020 년 12 월

위 원 장 이 원종 (인)

부 위 원 장 김 형 도 (인)

위 원 김 지 훈 (인)

위 원 정 성 훈 (인)

위 원 신 창 섭 (인)

Abstract

Cosmology of Light Scalar Dark Matters

Hyeontae Kim
Department of Physics and Astronomy
The Graduate School
Seoul National University

Despite the great success of ΛCDM supported by the precision cosmology, the CMB best fit value of the Hubble parameter has tension with the results from the local measurements. With more problems of CDM in small scales and null evidence of WIMPs in various experiments, alternative dark sector models with complex structures have been studied. This work focuses on the light scalars as dark matter candidates. There are two possibilities for scalar to have small mass naturally. As composite particles in an asymptotically free confining gauge theory, dark glueballs from a Yang-Mills gauge sector have mass around the confining scale. A pseudo-Goldstone boson is another possibility, and it can be incorporated as a form of a dark axion coupled to the gauge sector. Both dark glueballs and dark axion have non-trivial background evolution. In addition, initial isocurvature perturbation on the gluon temperature induce the density perturbation of the axion through the axion potential developed by the axion-gluon interaction. Finally, the dark glueballs as self-interacting sub-component dark matters can contribute to the gravo-thermal process of the formation of supermassive black holes.

Keywords: Dark matter, axion, glueball, self-interacting dark matter, density perturbations, supermassive black holes, gravo-thermal collapse
Student Number: 2013-22985

Contents

List of Figures

List of Tables

Chapter 1

Introduction

In 1929, Edwin Hubble measured the galaxy distances by observing Cepheid variables. Combining his results with the redshift associated with the galaxies observed by Vesto Slipher [1, 2], he obtained the proportionality between the distance and the receding velocity of the galaxies [3]. The linear relationship implies that the observed universe is expanding, which means that the physical length scale of the universe is being stretched as the cosmic time flows.

From late 1970s, systematic redshift surveys are developed and performed [4–6]. These surveys shows the distribution of the visible matters of the universe are statistically homogeneous and isotropic. The analysis on this large scale structure of the visible universe leads to the precise measurement of the local Hubble parameters and the evolution of the energy density of the universe that implies the energy composition of the universe. Along with some astrophysical observation such as the rotation curve of the galaxies, the existence of a dark matter, which seems to interact with the visible matters only gravitationally, became clear.

The observed homogeneous, isotropic, expanding universe is formulated by a solution to the Einstein equations, called the FRW metric. The 00 and ii components of the equations are called the Friedmann equations. They describe the relationship between the expansion of the universe and the energy constituents of the Universe.

One of the simplest and the most successful models on the energy composition of the universe has been the ΛCDM model. In this model, in addition to the standard model particles (photon, baryons, and neutrinos), a cold dark matter is introduced as a dark matter to explain the observed cosmological phenomena such as the formation of the large scale structure. To account the accelerating expansion of the current universe (Fig. 1.1), a dark energy is also introduced, which is realized as a cosmological constant Λ in the Einstein equations.

With the advance of the precision measurement of the cosmic microwave background (CMB) radiation, the analysis on the small anisotropy of order 10^{-5} on the photon temperature is developed [8]. The analysis strongly support the ΛCDM model. The model predicts the temperature power spectrum with great accuracy with just six model parameters. However, there are some tensions on the Hubble parameter H_0 and the density fluctuation power spectrum amplitude σ_8 between the CMB best fit value and the local measurements [9].

Along with ΛCDM cosmology, weakly interacting massive particle (WIMP) has been widely accepted as a cold dark matter candidate. The freeze-out relic abundance of a thermally produced dark matter whose mass is around the weak scale explains the observed relic abundance of the dark matter. This is called the WIMP miracle. However, the constraints on the WIMP cross section from the direct detection experiments have become severe, and the LHC experiments do not show any evidences of a new particle in this mass range.

With the cosmological tensions and the null evidence of WIMP, need for studies

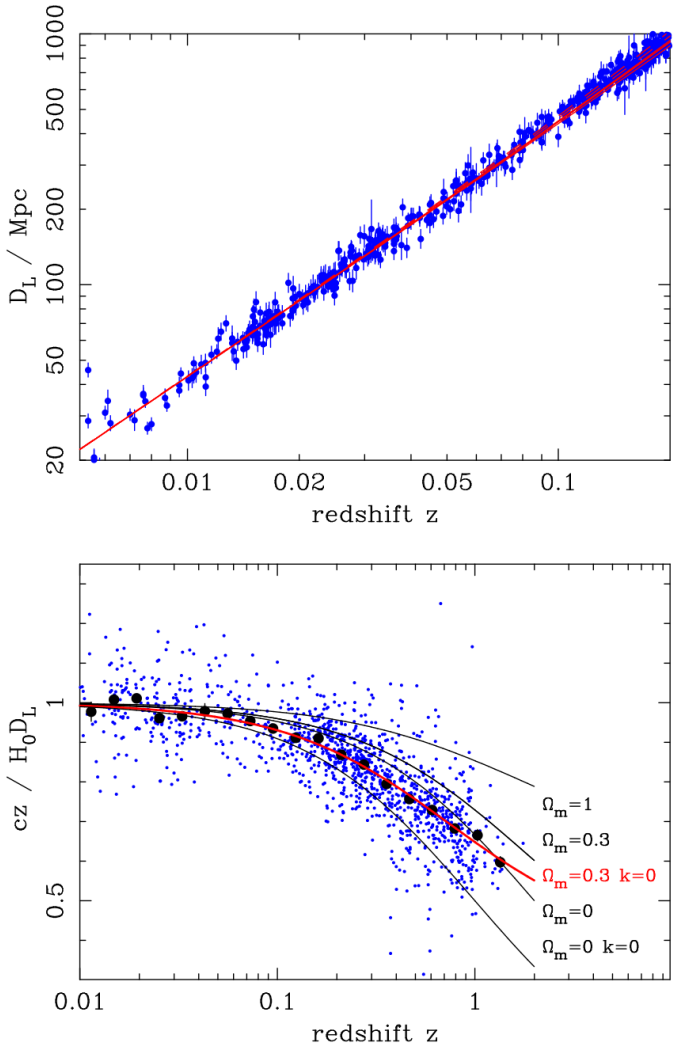

Figure 1.1 The type Ia supernova Hubble diagram, from Ref. [7]. In the second plot, the linear trend is divided. The black dots are median values in redshift bins.

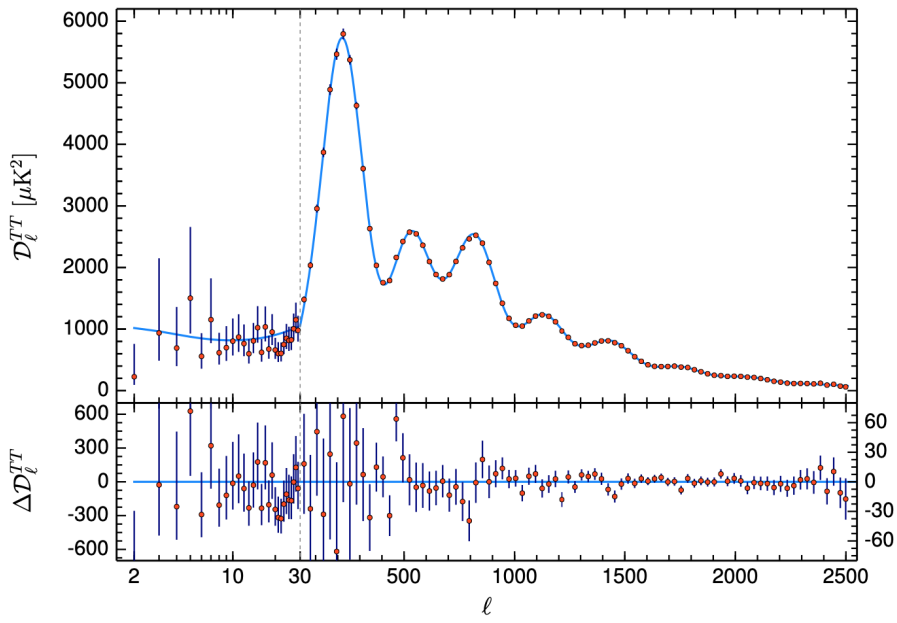

Figure 1.2 The observed temperature power spectrum (red) and the best-fit ΛCDM spectrum (light blue), from Ref. [8].

on various alternative dark matter models increases recently. There is no reason for dark matter to be simple or a single component. The dark matter can be multi-component, or, more generally, particles in a dark sector with complex structure like the standard model sector. Dark matter candidates in this rich structure can have wide spectrum of masses and spins. In this study, light scalar dark matter candidates are discussed. There are two natural cases that scalars have small mass. The first case is a composite particle in an asymptotically free gauge sector. Their mass is around the confining scale of the gauge sector. The second case is a pseudo-Goldstone boson. When the global symmetry is explicitly broken, the pseudo-Goldstone boson can have small mass proportional to the explicit symmetry breaking.

These two representative light scalars can be simultaneously incorporated in a

simple pure $SU(N)$ dark gauge sector. The former is dark glueballs in this gauge sector, and the latter is an axion-like particle coupled to the gauge sector. The dark glueballs are low energy degrees of freedom and possible dark matter candidates. The dark axion can be a cold dark matter candidates during its coherent oscillation phase. These two light scalar dark matter candidates in a simple gauge sector model have rich cosmological implications.

The dark axion coupled to the dark gauge sector itself can be a cold dark matter after it starts coherent oscillation. Since its potential is developed via its interaction with the dark gluon, the mass of the dark axion depends on the gluon temperature in the early universe. Because of the energy transfer from gluon to axion before the confining phase transition, the initial isocurvature perturbation induced by the initial fluctuation of the gluon temperature can produce the density perturbation of the axion.

In Chapter 2, we will review the standard Big Bang cosmology. The formalism for the expanding homogeneous isotropic universe, the consituents of the universe, and the cosmic inflation will be discussed. For the constituents of the universe, we focus on the ΛCDM cosmology and the WIMP dark matter. Then we will see the summary of the history of the universe and review some remaining cosmological problems. In Chapter 3, we will study the model of light scalar dark matters. We briefly review the axion cosmology and the QCD axion dark matter. Then we focus on the dark glueballs in a confining gauge sector and the dark axion coupled to the gauge sector as light scalar dark matters. We take into account the impact of the temperature dependent axion potential generated via the axion-gluon interaction in the dynamics of axion-gluon fluids. The density perturbation of the axion induced from the initial fluctuation of the gluon temperature will be calculated. We will also study the role of dark glueballs as sub-component self-interacting dark matters in the formation

process of the supermassive black holes. In Chapter 4, conclusion and discussion including some open questions will be provided.

Chapter 2

The Big Bang Cosmology

2.1 Formalism for Expanding Universe

The homogeneity and the isotropy, with the time-dependent spatial component of the metric to take account the expansion of the universe, leads to a solution to the Einstein equations, called the FRW metric. The line element of the FRW metric is given by

$$ds^2 = -dt^2 + a(t)^2 \left[\frac{dr^2}{1 - Kr^2} + r^2 d\Omega^2 \right] , \tag{2.1}$$

where $a(t)$ is called the scale factor, and the constant K describes the spatial curvature. $K = -1,\ 0,\ +1$ for open, flat, and closed universe, respectively. The time dependence of the scale factor is described by the Friedmann equations, the 00 and

ii component of the Einstein equations,

$$\left(\frac{\dot{a}}{a}\right)^2 + \frac{K}{a^2} - \frac{\Lambda}{3} = \frac{8\pi G}{3}\rho_{\rm tot} \ , \tag{2.2}$$

$$2\frac{\ddot{a}}{a} + \left(\frac{\dot{a}}{a}\right)^2 + \frac{K}{a^2} - \Lambda = -8\pi G p_{\rm tot} \ , \tag{2.3}$$

where Λ is the cosmological constant. Defining

$$\rho_\Lambda \equiv \frac{\Lambda}{8\pi G} \ , \ p_\Lambda \equiv -\rho_\Lambda, \tag{2.4}$$

then redefining $\rho_{\rm tot}$ and $p_{\rm tot}$ by absorbing Λ terms, the Hubble parameter is defined as

$$H^2 \equiv \left(\frac{\dot{a}}{a}\right)^2 = \frac{8\pi G}{3}\rho_{\rm tot} - \frac{K}{a^2} \ . \tag{2.5}$$

The Hubble parameter depends on the total energy density of the universe. Therefore, it is very important to figure out the nature of the constituents of the universe to understand the expansion history of the universe.

The continuity equation, $\nabla_\mu T^{\mu\nu} = 0$, can be seperated for each individual isolated constituent x, so

$$\dot{\rho}_x + 3H(1 + w_x)\rho_x = 0 \ , \tag{2.6}$$

where $w_x \equiv p_x/\rho_x$ is the equation of state. For a constant w_x, the energy density evolves as

$$\rho_x \propto a^{-3(1+w_x)} \ . \tag{2.7}$$

For a collisionless massive particle, $w_m = 0$, while $w_r = 1/3$ for a radiation and $w_\Lambda = -1$ for the cosmological constant (dark energy). Thus the energy density of the radiation drops faster than that of the cold dark matter as the universe expands.

Customarily, the current relic abundance of each component is expressed by

$$\Omega_x \equiv \frac{\rho_x({\rm today})}{\rho_{\rm crit}} \ , \tag{2.8}$$

where the critical density is defined as the total energy density of current flat universe,

$$\rho_{\rm crit} \equiv \frac{3H_0^2}{8\pi G} \ , \tag{2.9}$$

and H_0 is the Hubble parameter today.

For a universe with radiations, matters, and cosmological constant, the Hubble parameter at scale factor a is written as

$$H(a) = H_0\sqrt{\frac{\Omega_r}{a^4} + \frac{\Omega_m}{a^3} + \Omega_\Lambda + \frac{\Omega_K}{a^2}} \ , \tag{2.10}$$

where $\rho_K \equiv -\frac{3K}{8\pi G}$ and $\Omega_K \equiv \rho_K/\rho_{\rm crit}$. For a flat universe,

$$\sum_x \Omega_x = 1 \ . \tag{2.11}$$

Eq. (2.10) determines the evolution of the scale factor, i.e. the expansion of the universe. The conventional choice for the scale factor today is $a(\text{today}) = 1$.

2.2 The constituents of the universe

Current best estimate of the relic abundance of each component today [8] is

$$\Omega_r h^2 \sim 10^{-5} \ , \tag{2.12a}$$

$$\Omega_b h^2 \simeq 0.022 \ , \tag{2.12b}$$

$$\Omega_{\rm dm} h^2 \simeq 0.12 \ , \tag{2.12c}$$

$$\Omega_\Lambda h^2 \simeq 0.31 \ , \tag{2.12d}$$

$$\Omega_K h^2 \lesssim 10^{-2} \ , \tag{2.12e}$$

where the subscripts $r,\ b,\ \text{dm},\ \Lambda,\ K$ hold for the radiation, the baryons, the dark matter, the dark energy, and the curvature. h is defined by

$$H_0 = 100h \text{ km s}^{-1} \text{ Mpc}^{-1} \ . \tag{2.13}$$

As in Eq. (2.10), the energy density of each component evolves differently. Since the Hubble parameter depends on total energy density, it is important to figure out which component dominates the energy density of the universe. For example, though the radiations occupy very small fraction of the energy density of the universe today, they are dominant in the early universe in which the scale factor a is small. This era is called the radiation-dominated era (RD), On the other hand, the energy density of dark energy or cosmological constant is 70% of the total energy density of the universe today, but its contribution is negligible in the early universe. Between the radiation-dominated and dark energy-dominated era, there is matter-dominated era (MD) since the energy density of matter drops slower than that of radiation and faster than that of dark energy. In each era, the Hubble parameter is proportional to different power of the scale factor, and the evolution of density perturbation is also significantly different in each era. Depending on the particle properties of constituents, the evolution of the energy density and the Hubble parameter can be non-trivial. Therefore, it is important to figure out the nature of the constituents to understand the evolution history of the universe.

One of the simplest and the most successful model of the constituents of the universe is the ΛCDM model. It describes the flat universe with the standard model particles, a cold dark matter, and the cosmological constant. For the cold dark matter, no additional particle nature is assumed except its energy is dominated by its mass term. The evolution of the energy density of each component is depicted in Fig. 2.1. The energy density of the early universe is dominated by the photon. After $a = a_{\rm eq} = \Omega_r/\Omega_m \simeq 3 \times 10^{-4}$, the universe is dominated by the cold dark matter. The dark energy becomes dominant energy of the universe recently, $a \gtrsim 0.77$.

In the following subsections, the main constituents of the ΛCDM universe and their energy densities are briefly discussed. For a cold dark matter, we do not know

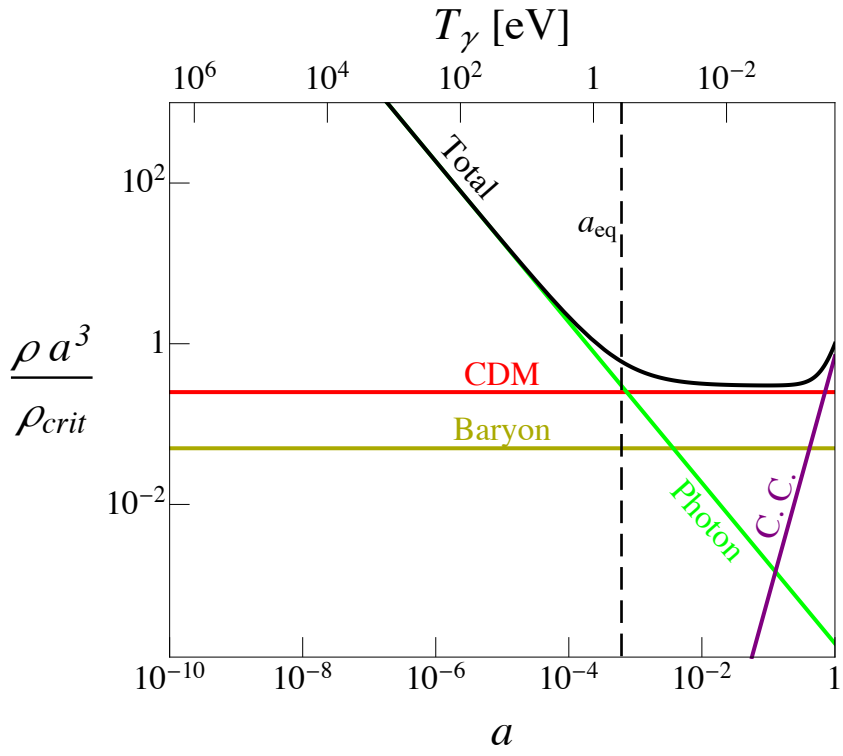

Figure 2.1 The evolution of the energy density of each component under ΛCDM cosmology, multiplied by a^3.

the true nature yet. Historically, the most widely accepted cold dark matter candidate had been WIMP dark matter, so it will be reviewed though the recent trend focuses on lots of alternative dark matter models.

2.2.1 Photons

We observe photons in the universe in the form of the cosmic microwave background. The measured temperature of the photon from the CMB precision measurements is $T_{\text{today}} = 2.726$ K [8]. Photon follows the Bose-Einstein distribution, so the

energy density of the photon is given by

$$\rho_\gamma = 2 \int \frac{d^3p}{(2\pi)^3} \frac{p}{e^{p/T} - 1} = \frac{\pi^2}{15} T^4 \ . \tag{2.14}$$

Since the energy density of radiations proportional to a^{-4}, the photon temperature is inversely proportional to the scale factor a. The current relic abundance of the photon is

$$\Omega_\gamma h^2 = 2.47 \times 10^{-5} \ , \tag{2.15}$$

which contributes very small portion of the energy density of the current universe.

2.2.2 Neutrinos

Though there is no direct observation on cosmic neutrino background, we know there are standard model neutrinos in our universe. The energy density of the standard model neutrinos with temperature T_ν is given by

$$\rho_\nu = 3 \times 2 \times \frac{7}{8} \times \frac{\pi^2}{30} T_\nu^4 \ , \tag{2.16}$$

where 3 is from the generations, 2 is from the neutrino and the antineutrino, and $\frac{7}{8}$ is from the Fermi-Dirac distribution. The neutrino temperature T_ν is different from that of the photon T. This is because the neutrinos decouples from the equilibrium with the rest of the standard model plasma slightly before e^+e^- annihilation happening at the temperature of order of the electron mass, which heats up the photons.

The total entropy of the standard model sector is conserved if there is no energy transfer between the standard model particle and the dark matter. The dominant contributions of the entropy density are from the radiations, so the entropy density before e^+e^- annihilation (at the time of the neutrino decoupling) is

$$s(a_{\rm before}) = \frac{2\pi^2}{45} \left[2 + \frac{7}{8}(4+6) \right] T_{\rm before}^3 \quad (T_\nu = T) \ , \tag{2.17}$$

accounting for the contributions from photons, electrons, positrons, and neutrinos. After the e^+e^- annihilation, the entropy density is

$$s(a_{\rm after}) = \frac{2\pi^2}{45}\left[2T_{\rm after}^3 + 6\times\frac{7}{8}T_{\nu,{\rm after}}^3\right] = \frac{2\pi^2}{45}\left[2\left(\frac{T_{\rm after}}{T_{\nu,{\rm after}}}\right)^3 + 6\times\frac{7}{8}\right]T_{\nu,{\rm after}}^3 \ . \tag{2.18}$$

Using the total entropy conservation and $T_\nu \propto 1/a$ after the decoupling,

$$\frac{T_\nu}{T} = \left(\frac{4}{11}\right)^{1/3} \ . \tag{2.19}$$

Therefore, the energy density of the neutrinos after e^+e^- annihilation is expressed by

$$\rho_\nu = 3\times\frac{7}{8}\left(\frac{4}{11}\right)^{4/3}\rho_\gamma \ . \tag{2.20}$$

The number density of a relativistic neutrino in thermal equilibrium is given by

$$n_{\nu_i} = \frac{3}{4}\frac{\zeta(3)}{\pi^2}T_\nu^3 \ , \tag{2.21}$$

and it drops proportional to a^{-3} after the neutrino temperature drops below its mass. Then the energy density of a single neutrino is $m_{\nu_i}n_{\nu_i}$. Since the number density is the same among different generations, sum of the relic abundance of the neutrinos is proportional to sum of the masses. The relic abundance of the neutrinos today is

$$\Omega_\nu h^2 \simeq \frac{\sum_i m_{\nu_i}}{94\ {\rm eV}} \ . \tag{2.22}$$

Current limit on the sum of the neutrino masses is

$$\sum_i m_{\nu_i} < 0.120\ {\rm eV}\ (95\%,\ {\rm TT,TE,EE+low\text{-}E+lensing+BAO}) \ , \tag{2.23}$$

from [8].

2.2.3 Baryons

The energy density of all ordinary matters in the standard model beside radiations is dominated by baryons since the protons and neurtons are much heavier than the

electrons. The baryons experience many different phases as the universe expands and the photon temperature drops. In the early hot universe, they form an ionized plasma and keep thermal equilibrium with photons. When the photon temperature drops to $\sim$ 1 MeV, the baryons form elements lighter than the helium (^{4}He).

The neutrons and the protons freeze out when the photon temperature is roughly 1 MeV at which the conversion rate via weak interaction become smaller than the Hubble expansion rate. In thermal equilibrium, the ratio of the number density of the proton to that of the neutron is

$$\frac{n_n^{\rm EQ}}{n_p^{\rm EQ}} = e^{(m_p - m_n)/T} \ . \tag{2.24}$$

After the freeze-out, this ratio remains constant ($\simeq 0.18$) until the production of the deuterium becomes efficient. This is the beginning of the Big Bang Nucleosynthesis. The equilibrium number density of the deuterium is approximately

$$\frac{n_D^{\rm EQ}}{n_b^{\rm EQ}} \sim \eta_b \left(\frac{T}{m_p}\right)^{3/2} e^{B_D/T} \ , \tag{2.25}$$

where $B_D = m_n + m_p - m_D$ is the binding energy of the deuterium, and

$$\eta_b \equiv \frac{n_b}{n_\gamma} = 6.0 \times 10^{-10} \left(\frac{\Omega_b h^2}{0.022}\right) \tag{2.26}$$

is the baryon to photon ratio. Defining the nucliation temperature $T_{\rm nuc}$ as the temperature at which the number density of the deuterium becomes comparable to that of the baryon, then $T_{\rm nuc} \simeq 0.07$ MeV. The neutron to proton ratio drops sharply at $T_{\rm nuc}$. Since the binding energy of the helium is larger than that of the deuterium, the heliums are formed immediately after the formation of the deuteriums. The abundance of the helium is roughly the half of the neutron at $T_{\rm nuc}$, so the mass fraction of the helium is given by

$$\left.\frac{4n(^4{\rm He})}{n_b}\right|_{T_{\rm nuc}} = \left.\frac{2n_n}{n_n + n_p}\right|_{T_{\rm nuc}} \simeq 0.22 \ . \tag{2.27}$$

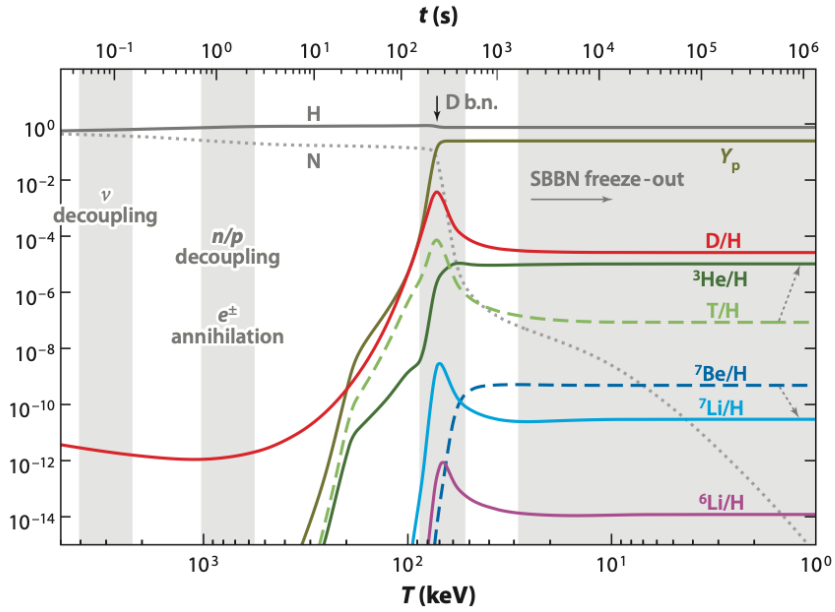

Figure 2.2 Change in mass fractions of light elements during the Big Bang Nucleosynthesis, from Ref. [10].

After $T_{\rm nuc}$, the remaining deuterium is elimiated via $\mathrm{D} + p \rightarrow {}^3\mathrm{He} + \gamma$. The deuterium eventually freezes out, and the remaining amount is sensitive to the baryon density, i.e. the baryon to photon ratio. The sensitivity is depicted in Fig. 2.3. Therefore, the observed fraction of the deuteriums today constrains the baryon relic abundance,

$$\Omega_b h^2 \simeq 0.022 \ . \tag{2.28}$$

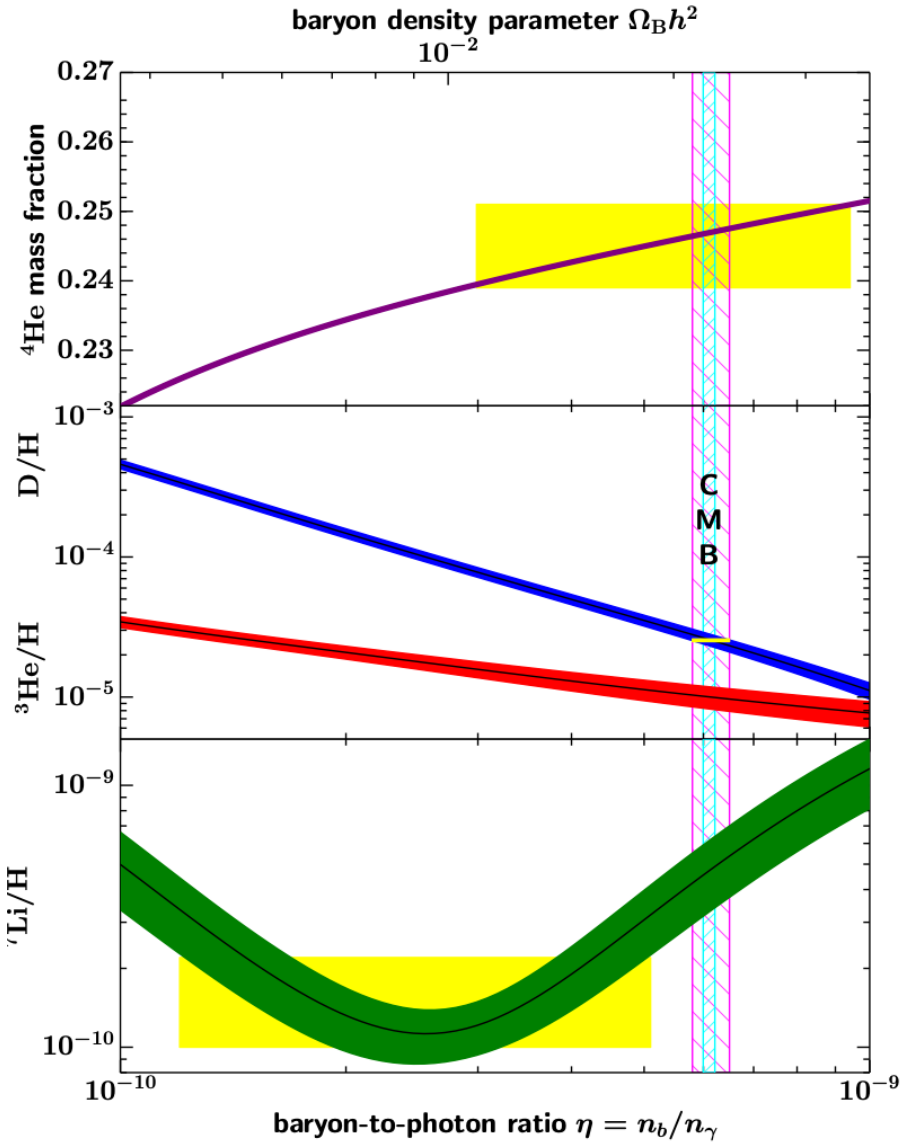

Figure 2.3 Fractions of light element as a function of the baryon-to-photon ratio, from Ref. [11]. The light blue CMB band indicates the CMB best fit value of the baryon density, and the wider magenta band indicates the range for the observed deuterium fraction to be consistent with the BBN prediction. The yellow boxes represent the observed light element abundances.

Among the remaining history of the baryon, the most important era is the time of recombination. As the universe is being cooled down, the Compton scattering becomes inefficient. Then the light nuclei and electrons form a stable bound state, starting from hydrogen atoms. This is called the recombination, and it happens at $T \sim 0.3$ eV or $z \sim 1100$, almost right after the matter-radiation equality. From this point the photon freely travels the universe. This photon is the cosmic microwave background.

2.2.4 Dark Matter

So far, the standard model particles are discussed. However, as mentioned earlier, they take up only about 5% of the energy density of our universe today. About six times larger portion of the energy density consists of dark matter. We know the energy fraction of dark matter today and the fact that at least the majority of the dark matter must be cold. We do not know other properties of dark matters such as spin, mass, and interactions. Historically, weakly interacting massive particles (WIMPs) have been considered as the most promising candidates of the cold dark matter. In this subsection, WIMPs will be mainly discussed as a cold dark matter candidate.

Suppose the dark matter has interaction with the standard model particles, and it is produced thermally from the standard model heat bath. Under the thermal equilibrium, the number density of a thermally produced dark matter follows the Boltzmann equation,

$$\frac{dn_\chi}{dt} + 3Hn_\chi = \langle\sigma v\rangle \left((n_{\chi,\mathrm{EQ}})^2 - n_\chi^2\right) \ , \tag{2.29}$$

where $n_{\chi,\mathrm{EQ}}$ is the equilibrium number density and $\Gamma_\chi \equiv \langle\sigma v\rangle n_\chi$ is the annihilation rate of the dark matter. During the radiation-dominated era, the Eq. (2.29) can also be expressed as

$$\frac{dY_\chi}{dx} = \frac{xs\langle\sigma v\rangle}{H(m_\chi)} \left(Y_{\chi,\mathrm{EQ}}^2 - Y_\chi^2\right) \ , \tag{2.30}$$

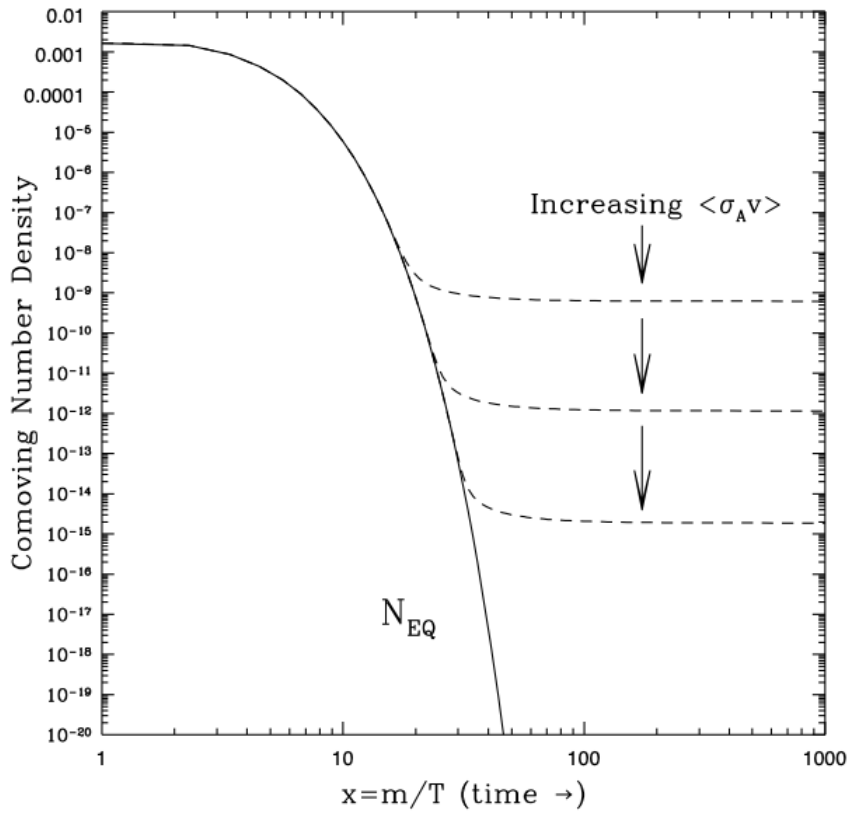

Figure 2.4 Evolution of the comoving number density of WIMP dark matter from [12].

where $Y_\chi \equiv n_\chi/s$ is the comoving number density of the dark matter, $x \equiv m_\chi/T \propto a$, and $H(m) \equiv H(x)x^2$. Here s is the total entropy of the universe, which is proportional to x^{-3}. The evolution of the comoving number density is described in Fig. 2.4.

The comoving number density freezes out when the interaction rate becomes smaller than the expansion rate, i.e.

$$H_{\rm FO} \simeq \Gamma_{\chi,{\rm FO}} \ . \tag{2.31}$$

The equilibrium comoving number density drops exponentially. The comoving number density is much larger than its equilibrium value after the freeze-out. After the freeze-

out, Eq. (2.30) can be expressed as

$$\frac{dY_\chi}{dx} = -\frac{\lambda}{x^2} Y_\chi^2 \quad (x \gg 1) \ , \tag{2.32}$$

where $\lambda \equiv \frac{m_\chi^3 \langle \sigma v \rangle}{H(m_\chi)}$. For s-channel annihilation, λ is a constant. It depends on temperature in some theories such as a case of dominant p-channel annihilation, but this does not change qualitative description. The solution to Eq. (2.32) is approximately

$$Y_{\chi,\mathrm{today}} \simeq \frac{x_{\mathrm{FO}}}{\lambda} \ . \tag{2.33}$$

By numerically solving Eq. (2.31) for x, $x_{\mathrm{FO}} \sim 20$. Thus the current relic abundance of the dark matter is

$$\begin{aligned} \Omega_\chi h^2 &= \frac{m_\chi s_{\mathrm{today}} Y_{\chi,\mathrm{today}}}{\rho_{\mathrm{crit}}} h^2 \sim \frac{10^{-26}\ \mathrm{cm}^3/\mathrm{s}}{\langle \sigma v \rangle} \\ &\sim 0.1 \left(\frac{0.01}{\alpha} \right)^2 \left(\frac{m_\chi}{100\ \mathrm{GeV}} \right)^2 \ . \end{aligned} \tag{2.34}$$

Eq. (2.34) gives correct dark matter relic abundance for weak-scale dark matter. This is called the WIMP miracle. Since weak-scale dark matters are also well motivated by the supersymmetric models, WIMP model had been a dominant paradigm for a dark matter candidates.

However, recent studies on the dark matter are not inclined to WIMPs. The constraints on the WIMP-nucleon interaction have become severe as in Fig. 2.5. Moreover, there is no evidence of a new particle in the weak scale in the LHC experiments.

2.3 The Cosmic Inflation

In the previous sections, some non-trivial observational properties of the universe are briefly mentioned. One of them is homogeneity or isotropy of the universe. The observation on the cosmic microwave background and the galaxy surveys show the

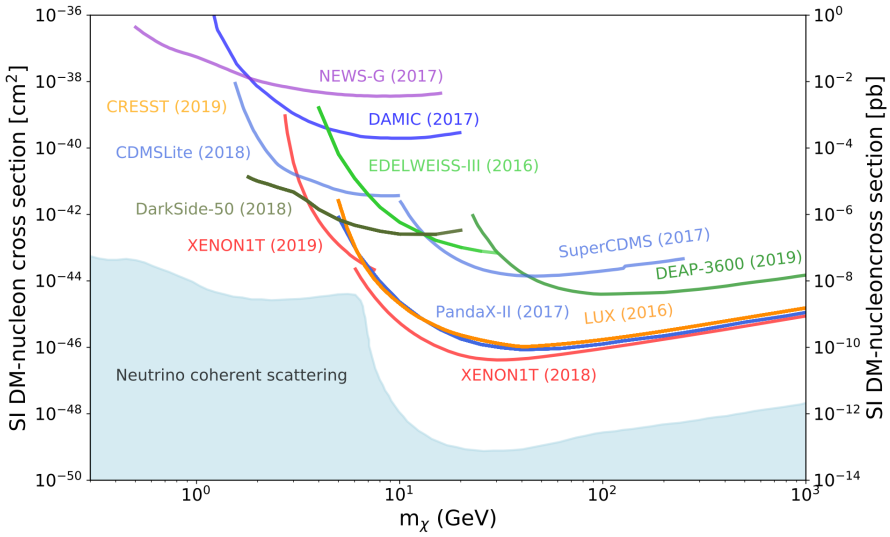

Figure 2.5 A compilation of WIMP-nucleon spin-independent cross-section limits, from Ref. [7].

universe is statistically homogeneous and isotropic. The isotropy of CMB can be explained if the universe was in thermal equilibrium at some point in time before the recombination. The maximum size of the region in thermal contact at the time of recombination is given by the distance that light travels until the time of recombination. The corresponding comoving distance is

$$r_{\rm rec} = \int_0^{t_{\rm rec}} \frac{dt}{a(t)} \simeq \frac{2}{\sqrt{\Omega_m} H_0} \frac{1}{\sqrt{1+z_{\rm rec}}} \ . \tag{2.35}$$

On the other hand, the size of the universe that can be observed via the CMB is the distance that light travel from the time of recombination to today.

$$r_{\rm obs} = \int_{t_{\rm rec}}^{t_0} \frac{dt}{a(t)} \simeq \frac{2}{\sqrt{\Omega_m} H_0} \ . \tag{2.36}$$

Thus the corresponding angle to the size of the causally connected patch is

$$\theta = \frac{r_{\rm rec}}{r_{\rm obs}} \simeq 0.03 \simeq 2^\circ \ . \tag{2.37}$$

This means that the thermal equilibrium cannot explain the observed isotropy of the CMB. This is the horizon problem in the Big Bang cosmology.

The comoving horizon at time t is

$$r = \int_0^t \frac{dt'}{a(t')} = \int_0^a \frac{d\ln a'}{a'H(a')} \ . \tag{2.38}$$

The integrand $1/(aH)$ is called the comoving Hubble radius, which represents the comoving distance that light travels within unit change in the order of the scale factor. The horizon problem can be resolved by introducing an early era in which the comoving Hubble radius decreases. We expect that causally connected region in the early universe exits the comoving hubble radius during this era, and then it re-enter the horizon during subsequent radiation-dominated era or matter-dominated era. The condition for this era is then

$$\frac{d}{dt}\left(\frac{1}{aH}\right) = -\frac{\ddot{a}}{\dot{a}^2} < 0 \ . \tag{2.39}$$

Therefore, in this era, the expansion of the universe is accelerating, so it is called the inflationary era. The condition in Eq. (2.39) is equivalent to

$$\frac{d}{da}\left(\frac{1}{aH}\right) < 0 \ \Rightarrow \ \frac{d\ln H}{d\ln a} > -1 \ . \tag{2.40}$$

With Eq. (2.5) and (2.7),

$$w_{\rm tot} \equiv \frac{p_{\rm tot}}{\rho_{\rm tot}} < -\frac{1}{3} \ . \tag{2.41}$$

For the observed universe to be in thermal equilibrium before the inflation, the comoving Hubble radius at the beginning of the inflation must be larger than that today. Ignoring short matter- and dark energy-dominated era, the universe is mostly in the radiation dominated era after the inflation. Then the ratio of the comoving Hubble radius today to that at the end of the inflation is

$$\frac{a_{\rm end}H_{\rm end}}{a_0H_0} \simeq \frac{a_0}{a_{\rm end}} \simeq \frac{T_{\rm end}}{T_0} \ . \tag{2.42}$$

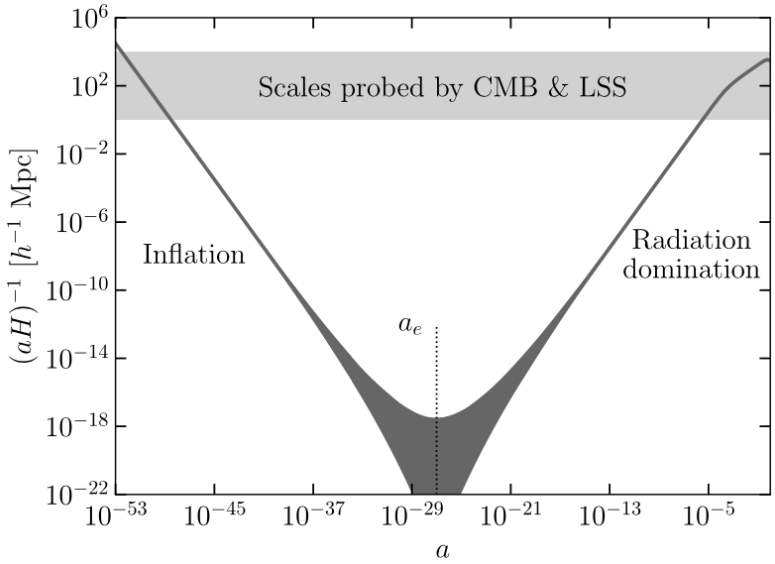

Figure 2.6 The comoving Hubble radius and the relevant comoving scales of LSS and CMB during and after the inflation, from Ref. [14].

Current constraint on the Hubble parameter during the inflation is

$$\frac{H_{\rm end}}{M_P} < 2.5 \times 10^{-5} \quad (95\%\ \text{C.L.}) \ , \tag{2.43}$$

from [13]. If the photon dominates the energy density of the universe after the inflation, $H_{\rm inf} \simeq T_{\rm end}^2/M_P$. Taking the marginal value,

$$\frac{a_{\rm end}H_{\rm end}}{a_0H_0} \simeq \frac{a_0}{a_{\rm end}} \simeq 10^{27} \simeq e^{62} \ . \tag{2.44}$$

Therefore, the comoving Hubble radius must decrease at least 60 e-folds during the inflation.

One of the possible mechanism of the inflation is one using a single scalar field. Suppose there is an era in which the energy density of the universe is dominated by a scalar field $\phi_{\rm inf}$ with its potential $V(\phi)$.

$$-\frac{\mathcal{L}}{\sqrt{-g}} = \frac{1}{2}\partial_\mu\phi_{\rm inf}\partial^\mu\phi_{\rm inf} - V(\phi_{\rm inf}) \ . \tag{2.45}$$

$\phi_{\rm inf}$, called inflaton, follows the equation of motion,

$$\ddot{\phi}_{\rm inf} + 3H\dot{\phi}_{\rm inf} + V_{,\phi_{\rm inf}} = 0 \ . \tag{2.46}$$

Its energy density and pressure are 00 and ii components of the energy-momentum tensor, derived from the Lagrangian density for a canonical scalar field. They are given by

$$\rho = \frac{1}{2}\dot{\phi}_{\rm inf}^2 + V(\phi_{\rm inf}) \ , \tag{2.47}$$

$$p = \frac{1}{2}\dot{\phi}_{\rm inf}^2 - V(\phi_{\rm inf}) \ . \tag{2.48}$$

If the potential energy is much larger than the kinetic energy, then $w \simeq -1$, satisfying the condition in Eq. (2.41). Large e-fold number can be archived by 'slow-roll' approximation,

$$\dot{\phi}_{\rm inf}^2 \ll V(\phi_{\rm inf}) \ , \ |\ddot{\phi}_{\rm inf}| \ll |V_{,\phi_{\rm inf}}| \ . \tag{2.49}$$

Then

$$3H\dot{\phi}_{\rm inf} \simeq -V_{,\phi_{\rm inf}} \ , \ H^2 \simeq \frac{8\pi}{3M_P^2}V \ . \tag{2.50}$$

From Eq. (2.49) and (2.50),

$$\frac{1}{M_P^2}\left(\frac{V_{,\phi_{\rm inf}}}{V}\right)^2 \ll 1, \tag{2.51}$$

so the e-fold number calculated as

$$N \equiv \ln\frac{a(t_{\rm end})}{a(t_{\rm start})} = \int_{t_{\rm start}}^{t_{\rm end}} H dt \simeq \frac{8\pi}{M_P^2}\int_{\phi_{\rm end}}^{\phi_{\rm start}} \frac{V}{V_{,\phi_{\rm inf}}} d\phi_{\rm inf} \tag{2.52}$$

can be very large. Therefore, the cosmic inflation can resolve the horizon problem.

The inflation can solve another problem, called the flatness problem. As in Eq. (2.12), the universe we observe actually seems to be flat. Since the curvature term proportional to a^{-2}, $\Omega_K(a)$ in the early universe is even smaller than its current value. For example, $\Omega_K/\Omega_r < 10^{-16}$ at BBN epoch. The Big Bang cosmology does

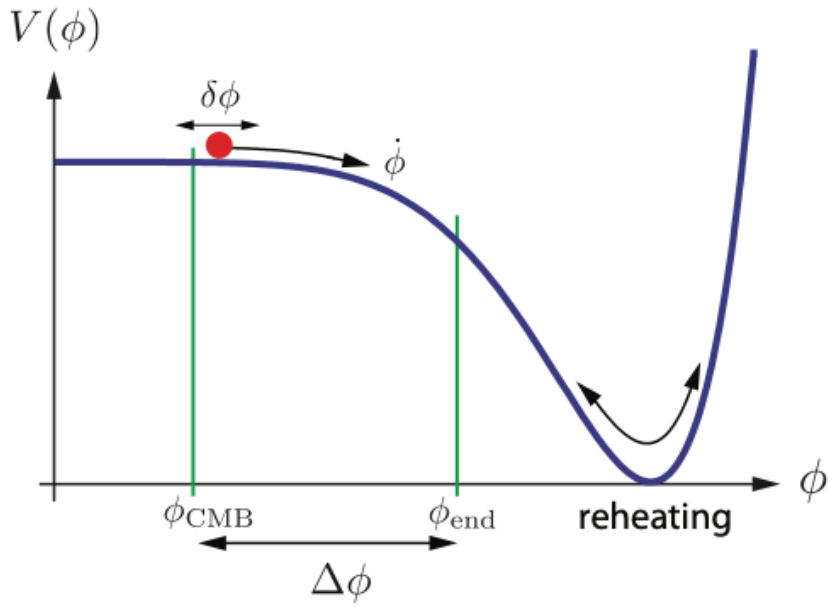

Figure 2.7 Example of inflaton potential for slow-roll inflation, from Ref. [15]. The subscript CMB and end indicate the moment which the CMB fluctuation is created and the inflation end, respectively.

not predicts this fine-tuning without the cosmic inflation. Since $\Omega_K(a) \propto a^{-2}$, if there is an inflationary era,

$$\frac{\Omega_K(a_{\rm end})}{\Omega_K(a_{\rm start})} \simeq \left(\frac{a_{\rm start}}{a_{\rm end}}\right)^2 = e^{-2N} \ . \tag{2.53}$$

Therefore, the inflation explains smallness of Ω_K after the inflation.

In the inflationary model, the ordinary particles such as photons are produced by the decay of inflation. This process is called the reheating process, and it happens right after the inflation ends.

2.4 Summary

As mentioned earlier, the ΛCDM universe consists of the photons, the baryons, the cold dark matter, and the cosmological constant. The energy portions of these constituents in the early universe are different from the values now since they evolve in different manner as the universe expands. The expansion of the universe or the evolution of the Hubble parameter is determined by which component dominates the energy density of the universe.

In the very early universe, the universe we observe today was very small and thermalized. At $H \lesssim 10^{-5} M_P$, the cosmic inflation takes places, diluting all matters, radiations, and curvature except the scalar field called the inflaton. During this era, the scales we observe exit the comoving Hubble radius. The inflation lasts until $T \lesssim 10^{16}$ GeV or $a \gtrsim 10^{-30}$. After the inflation, the inflaton dominantly decays to the standard model particles. The photons are produced in this reheating era, dominating the total energy of the universe.

Though the photons are dominant component in this era, there are baryons coupled to the photons. These baryons starts to form the light nuclei at $T \sim 1$ MeV or $a \sim 10^{-11}$. This is called the Big Bang Nucleosynthesis. The decoupling of these elements from the photon happens much later, at $T \sim 0.3$ eV or $a \sim 10^{-3}$. Since the light elements form neutral atoms, we call this the recombination. The recombination happens right after the matter-radiation equality at $T \sim 1$ eV. The photons travel the universe freely, and we observe these photons in the form of cosmic microwave background.

During the matter dominant era, the large scale structure grows via gravitational interaction. The dark matter plays an important role in here since they form gravitational potential dominantly. At $a \sim 0.1$, stars and galaxies start to form. Very

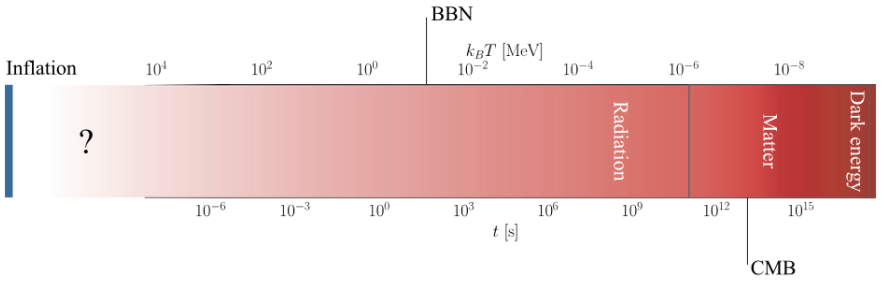

Figure 2.8 A history of the universe, from Ref. [14].

recently, the universe becomes the dark energy-dominated era, and the expansion is accelerating.

2.5 Remaining Cosmological Problems

In the previous sections, the Big Bang cosmology with ΛCDM model and inflation are discussed. It explains most of the cosmological phenomena and manages to resolve many theoretical problems. However, there are still some observational issues with the ΛCDM cosmology and the WIMP dark matter. These issues are driving studies on the alternative cosmology models. These issues are briefly covered in the following subsections.

2.5.1 The Hubble Tension

The precision measurement of the cosmic microwave background radiation shows that the CMB temperature power spectrum is extremely well fitted based on the ΛCDM model. However, there is tension between the Hubble parameters from dif-

ferent observations. The base-ΛCDM best fit value from the CMB is $H_0 \simeq 67.4 \pm 0.5$ km/s/Mpc (68% C.L.) [8], while the combination of local direct measurements shows $H_0 \simeq 73.3 \pm 0.8$ (68% C.L.) [16]. The tension between two is 6.1σ.

The Hubble tension is one of the reason that the ΛCDM model has been questioned. In this context, many alternative dark matter or dark energy models are studied recently. One of the possible resolution is changing the radiation degrees of freedom at the time of recombination. In the next chapter, glueballs in a dark confining gauge sector will be discussed as dark matter candidates. These glueballs can mildly reduce the Hubble tension since their number-changing self-interaction causes pressure that make glueballs behave like warm dark matter component.

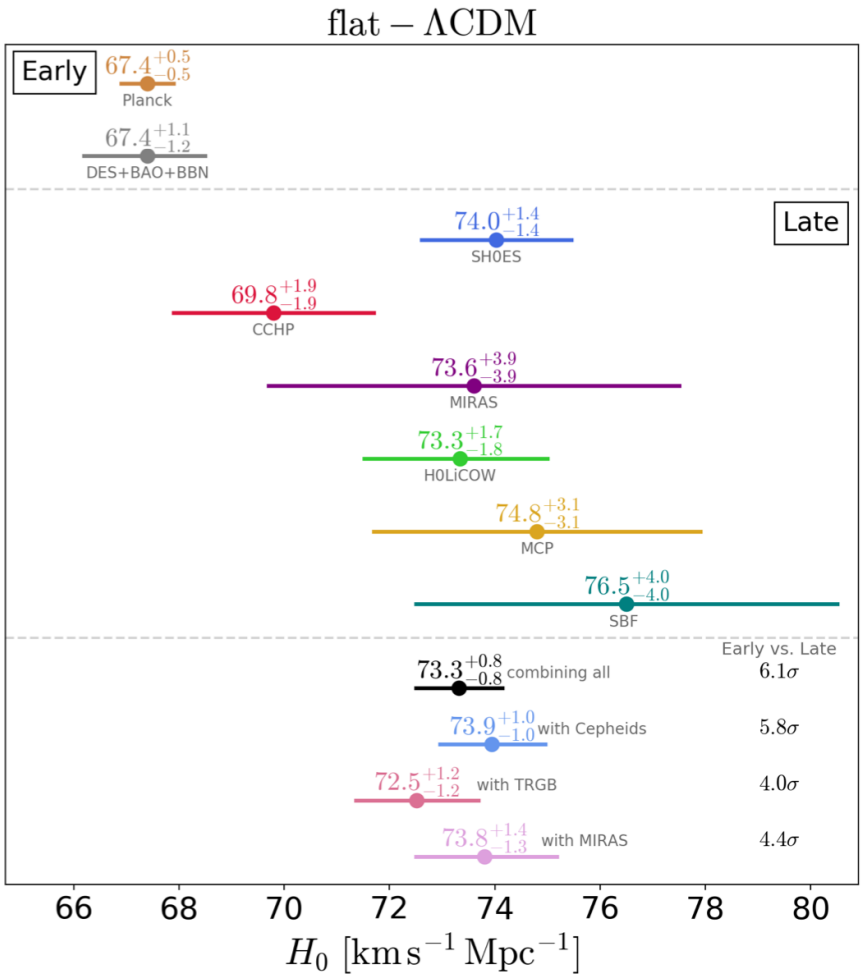

Figure 2.9 The tensions on the current Hubble parameter between various observations, from Ref. [16].

2.5.2 The Problems in Small Scale

Most of the cosmological N-body simulations on the dark matter halo show that the density profile of CDM halo can be characterized by a power law slope [17–19]. Simulations suggest that the inner halo density distribution is well described by profile expressed as

$$\rho(r) = \frac{\rho_s}{(r/R_s)^{\alpha}(1 + r/R_s)^{3-\alpha}} \ , \tag{2.54}$$

where ρ_s is related to the critical density of the universe, and R_s is the characteristic radius of the halo. The slope α varies among simulations. Typically $0.7 \leq \alpha \leq 1.5$, and $\alpha = 1$ for the NFW profile.

On the other hand, the observations on the dwarf galaxies indicate the existence of constant density or mildly cuspy dark matter cores [20]. The discrepancy between the observation and the simulation is called the core-cusp problem. Many solutions on the core-cusp problem have been studied recently such as baryonic feedback models, fuzzy dark matter models, or self-interacting dark matter models.

Another discrepancy between cosmological N-body simulations and observations is the number of dwarf galaxies. The simulation with cold dark matter generates more dwarf galaxies than observations. For example, the observation of 38 dwarf galaxies on the Local Group is much less than the prediction of simulations, which is about 500 satellite galaxies for the Milky Way [21, 22]. This is called the missing satellites problem.

One possible reason for the missing satellites problem is that the satellite galaxies are too faint to be observed. Actually, many faint Milky Way satellite galaxies have been discovered. However, the satellite galaxies are much heavier in the N-body simulations than observed satellite galaxies. This is the too-big-to-fail problem.

Finally, the observatios of supermassive black holes with mass $\sim 10^9 M_{\odot}$ near

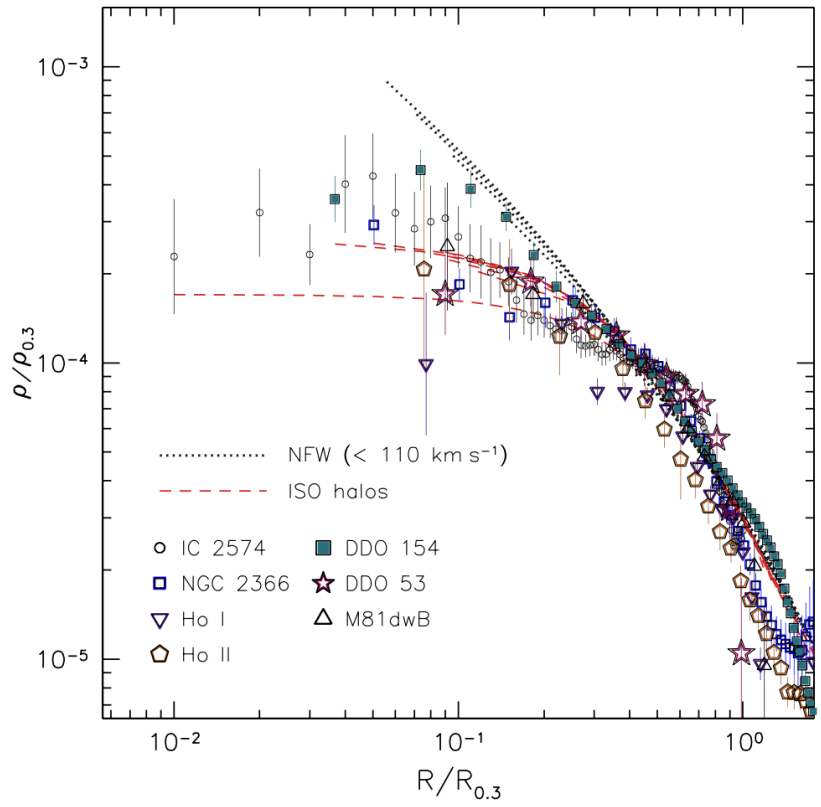

Figure 2.10 The observation on the central density profile of dwarf galaxies, from Ref. [20].

$z = 7$ are not explained by the standard ΛCDM cosmology. The upper bound on the mass of supermassive black holes can be imposed by the Eddington limit.

$$M_{\rm SMBH} \leq M_{\rm seed} e^{\frac{t_{\rm obs} - t_{\rm seed}}{t_{\rm Sal}}} \ , \tag{2.55}$$

where $t_{\rm Sal}$ is the Salpeter time, which is the maximum e-folding rate via gas accretion. The typical value is $t_{\rm Sal} \simeq 45$ Myr. For $z = 7$, the age of universe is about 750 Myr after the Big Bang. For a black hole with mass $M_{\rm SMBH} \simeq 10^9 M_\odot$ to be observed at $z \simeq 7$, the mass of the seed black hole should be larger than $100 M_\odot$ even though the growth of the black hole follows the Eddington limit. The standard prediction of the mass of

seed black holes formed by supernova explosion of early stars is $M_{\rm seed} \sim 5 - 20 M_{\odot}$, which is not sufficient to explain the mass of the observed supermassive black holes.

Chapter 3

Axion Dark Matter and Confining Dark Sector

3.1 Motivation

As we discussed in Sec. 2.5, there are still some limits on the standard ΛCDM cosmology and the WIMP dark matter. Recent cosmological studies are more focusing on alternative models that resolving these problems. For example, the Hubble tension can be reduced by introducing warm dark matter such as sterile neutrinos. Because of non-zero pressure, its energy density drops faster than that of CDM as the universe expands. This implies more energy density at the time of recombination, increasing derived Hubble parameter. Another example is a fuzzy dark matter as a solution to the core-cusp problem. Ultra-light axion is considered as a fuzzy dark matter. Because

of its coherent oscillation, the background energy density evolves like that of cold dark matter. However, this dark matter prevents the formation of small scale structure with size smaller than its de Brogile wavelength. For $m \sim 10^{-21}$ eV, the corresponding de Brogile wavelength is about the size of core of observed dwarf galaxies, so it prevents the cuspy profile predicted by ordinary CDM scenario.

Various dark matter models give similar or different implications on each cosmological problem. Since there is no direct evidence on the properties of dark matter beside from gravitational interaction, recent studies seek to solve many cosmological problems simultaneously. Following this trend, models of dark sector with more complex structure have been recently developed. Constituents in this complex structure can have wide spectrum of masses and spins.

In this study, we focus on the case of light scalar dark matters. While it is natural for fermions to have small mass, it is very unnatural to consider light scalars if there is no reason for it. There are two representative light scalars. The first case is a composite dark matter in a confining gauge sector. The mass of the composite dark matter is given by the confining scale of the gauge sector, which is the point where the running coupling diverges. Another light scalar with natural small mass is a pseudo-Goldstone bosons whose tiny mass is associated with the spontaneous breaking of global symmetry. A pseudo-Goldstone boson, as a form of an axion-like particle, can be incorporated in the confining dark gauge sector. This axion-like particle or (dark) axion coupled to this gauge sector gets its mass from the interaction with the gluon. In the following sections, the background evolution of each light scalar and their interplay will be studied.

3.2 Cosmology of Axion

More strict constraints on the interaction cross section between the standard model particles and the WIMP and no evidence of any supersymmetric particles in LHC experiments, along with mentioned cosmological problems in the previous section, require the development of alternative dark matter models. One of possible dark matter candidates is QCD axion or axion-like particles.

3.2.1 The Strong CP Problem and QCD Axion

Axion was introduced as a solution to the strong CP problem. The QCD Lagrangian contains a topological CP violating term

$$\mathcal{L}_{\theta_{\rm QCD}} = \frac{\theta_{\rm QCD}}{32\pi^2}{\rm Tr}G_{\mu\nu}\tilde{G}^{\mu\nu} \ . \tag{3.1}$$

The notation Tr for the trace over the adjoint representation of $SU(3)$ will be omitted afterward. This term yields electric dipole moment of the neutron,

$$d_n \simeq 3.6 \times 10^{-16}\theta_{\rm QCD} e \text{ cm} \ . \tag{3.2}$$

Recent constraint on the neutron electric dipole moment is $|d_n| < 1.8 \times 10^{-26} e$ cm (95% C.L.) [PRL124,081803]. This implies small $\theta_{\rm QCD}$,

$$\theta_{\rm QCD} \lesssim 10^{-10} \ . \tag{3.3}$$

The observed CP-violation of the electroweak sector implies that $\theta_{\rm QCD}$ could be $\mathcal{O}(1)$. For small value of measured $\theta_{\rm QCD}$, it must be canceled precisely by the quark mass

$$\theta_{\rm QCD} = \tilde{\theta}_{\rm QCD} + {\rm ArgDet}M_u M_d \ , \tag{3.4}$$

so the smallness of measured $\theta_{\rm QCD}$ requires fine tuning.

The small $\theta_{\rm QCD}$ is explained by introducing an anomalous symmetry $U(1)_A$,

$$u \to e^{i\alpha} u \ , \quad d \to e^{i\alpha} d \ , \quad \theta_{\rm QCD} \to \theta_{\rm QCD} - 2\alpha \ , \tag{3.5}$$

explicitly broken only by the QCD anomaly,

$$S \to S + \int \partial^4 x \frac{\alpha}{32\pi^2} G_{\mu\nu} \tilde{G}^{\mu\nu} \ . \tag{3.6}$$

The topological term does not affect the classical equation of motion, but it changes vacuum structure. The vacuum energy depends on $\theta_{\rm QCD}$, given by

$$E_{\rm vacuum} \propto \cos \theta_{\rm QCD} \ . \tag{3.7}$$

Introducing an axion field ϕ that couples to $G\tilde{G}$ by

$$\mathcal{L}_\phi \supset \frac{1}{32\pi^2} \frac{\mathcal{C}\phi}{f_a} G_{\mu\nu} \tilde{G}^{\mu\nu} \ , \tag{3.8}$$

and absorbing $\theta_{\rm QCD}$ by the shift symmetry of ϕ, the vacuum energy is

$$E_{\rm vacuum} \propto \cos\left(\frac{\mathcal{C}\phi}{f_a}\right) \ . \tag{3.9}$$

The vacuum energy can be minimized since it depends on a dynamical field. The coefficient $\mathcal{C}$ is called the color anomaly, and it must be integer since the axial field ϕ must have a symmetry under $\phi \to \phi + 2\pi f_a$. The color anomaly sets the number of vacua in $[0, 2\pi f_a]$, so it is called the domain wall number $\mathcal{C} = N_{\rm DW}$. $N_{\rm DW} = 1$ for following discussions.

Below the QCD confinement scale, the axion potential induced by QCD instanton is

$$V(\phi) = m_u \Lambda_{\rm QCD}^3 \left[1 - \cos\left(\frac{\phi}{f_a}\right)\right] \ . \tag{3.10}$$

Expanding it around the potential minimum,

$$m_a^2 \simeq \frac{\Lambda_{\rm QCD}^4}{f_a^2} \ . \tag{3.11}$$

Above the QCD confinement scale, the axion mass depends on the temperature via non-perturbative effect.

3.2.2 Axion Dynamics under the FRW Metric

In the previous section, we consider the QCD axion. In general, it is possible to consider an axion-like particles (ALP) coupled to a gauge sector. The dynamics described in this section can be applied these kinds of models. The minimal Lagrangian for axion (or ALP) coupled to a gauge sector is

$$\frac{\mathcal{L}_\phi}{\sqrt{-g}} = \frac{1}{2}(\partial\phi)^2 + V(\phi) \ . \tag{3.12}$$

From the energy momentum tensor, energy density and pressure of the axion are given by

$$\rho_a = \frac{1}{2}\dot{\phi}^2 + \frac{1}{2}m_a^2\phi^2 \ , \quad p_a = \frac{1}{2}\dot{\phi}^2 - \frac{1}{2}m_a^2\phi^2 \ . \tag{3.13}$$

The equation of motion for background field ϕ is

$$\ddot{\phi} + 3H\dot{\phi} + m_a(T)^2\phi = 0 \ . \tag{3.14}$$

For an axion with initial misalignment angle,

$$\phi_i = f_a\theta_i \ , \quad \dot{\phi}_i = 0 \ . \tag{3.15}$$

If the second term in Eq. (3.14) dominates the third term, the axion field rolls slowly. The potential energy is much larger than the kinetic energy in this limit. On the other hand, if the third term dominates the second term, the axion starts oscillating. Averaging over the fast oscillation, the kinetic energy is equal to the potential energy. The conventional pivot that distinguishes two region is is $m_a = 3H$. Thus the equation of state is given by

$$w_a = \begin{cases} -\frac{1}{3} & \text{if } H \gg m_a \ , \\ 0 & \text{if } H \ll m_a \ . \end{cases} \tag{3.16}$$

Therefore, the axion (or ALP) plays a role of dynamical dark energy before it starts the oscillation, and it behaves as a cold dark matter during the oscillation phase.

3.2.3 Energy Density of the Axion Dark Matter

Now we define the quantity N_a as

$$N_a(a) = \frac{\rho_a(a)a^3}{m_a(T(a))}. \tag{3.17}$$

From Eq. (3.13) and (3.14), N_a satisfies

$$\dot{N}_a + \left(3H + \frac{\dot{m}_a}{m_a}\right)\langle w_a\rangle N_a = 0 \ . \tag{3.18}$$

During the oscillation phase $\langle w_a\rangle = 0$, so N_a is conserved. The energy density of the axion after the oscillation starts is

$$\rho_a(a) \simeq \rho_a(a_{\rm osc})\frac{m_a}{m_a(a_{\rm osc})}\left(\frac{a_{\rm osc}}{a}\right)^3 \ , \tag{3.19}$$

where $a_{\rm osc}$ is the scale factor at the time when the oscillation starts, and

$$\rho_a(a_{\rm osc}) \simeq \frac{1}{2}m_a(a_{\rm osc})^2 f_a^2\theta_i^2 \ . \tag{3.20}$$

The expression for the relic abundance of axion depends on whether the oscillation starts before or after the axion mass is saturated. For QCD axion, the relic abundance is given by

$$\Omega_a h^2 \simeq \begin{cases} 2\times 10^4 \left(\frac{f_a}{10^{16}\ {\rm GeV}}\right)^{7/6}\theta_i^2 & \text{for } a_{\rm osc} < a_{\rm conf} \ , \\ 5\times 10^3 \left(\frac{f_a}{10^16\ {\rm GeV}}\right)^{3/2}\theta_i^2 & \text{for } a_{\rm osc} > a_{\rm conf} \ , \end{cases} \tag{3.21}$$

where $a_{\rm conf}$ is the scale factor at QCD confinement. Considering the domain wall problem, the axion decay constant f_a should be larger than the inflation scale. Therefore, for the QCD axion to be the cold dark matter in our universe, the initial misalignment angle should be small, $\theta_i \ll 10^{-2}$. Axion-like particles that are coupled to other (dark) gauge sector can avoid this small initial misalignment angle condition, depending on the confining scale of the gauge sector. More detailed dynamics, relic abundance, and perturbations related to the axion-like particle (or dark axion) coupled to the dark gauge sector will be discussed in Section 3.3.

3.3 Dark Axion Coupled to a Confining Dark Sector

3.3.1 Description of the Model

Our starting Lagrangian of dark sector is composed of the ultra-light axion ϕ whose field range is $2\pi f_a$, and the dark gauge symmetry with the confinement scale Λ ($\Lambda \ll f_a$). The coupling between the axion and the dark gauge bosons are given as

$$-\frac{\mathcal{L}_h}{\sqrt{-g}} = \frac{1}{2}(\partial_\mu \phi)^2 + \frac{1}{4}(G^a_{\mu\nu})^2 + \frac{g^2\phi}{32\pi^2 f_a} G^a_{\mu\nu}\tilde{G}^{a\mu\nu}, \tag{3.22}$$

where $G^a_{\mu\nu}$ is the dark gluon field strength and g denotes the dark gauge coupling. For illustration, we take $SU(N)$ as the dark gauge group in our set-up. Below the confinement scale, the dynamics of the gauge fields can be described by the composite bosons, the glueballs. Considering the lightest glueball φ_g, the effective Lagrangian of φ_g can be expanded in $(4\pi/N)(\varphi_g/m_g)$ [23–26]

$$\begin{aligned} -\frac{\mathcal{L}_{h\text{eff}}}{\sqrt{-g}} &= \frac{1}{2}(\partial_\mu\phi)^2 + V(\phi) + \frac{1}{2}(\partial_\mu\varphi_g)^2 + \frac{1}{2}m_g^2\varphi_g^2 \\ &\quad + \frac{a_1}{3!}\Big(\frac{4\pi}{N}\Big) m_g \varphi_g^3 + \frac{a_2}{4!}\Big(\frac{4\pi}{N}\Big)^2 \varphi_g^4 \\ &\quad + \frac{a_3}{5!}\Big(\frac{4\pi}{N}\Big)^3 \frac{\varphi_g^5}{m_g} + \cdots, \end{aligned} \tag{3.23}$$

where m_g is the glueball mass of $\mathcal{O}(\Lambda)$. The axion also gets a scalar potential by the gluodynamics, which can be written as a power series in $(\phi/Nf_a)^2$ around its minimum ($\phi = 0$) [27, 28]

$$\begin{aligned} V(\phi) &= N^2\Lambda^4\Big(\frac{c_1}{2}\frac{\phi^2}{N^2 f_a^2} + \frac{c_2}{4!}\frac{\phi^4}{N^4 f_a^4} + \cdots\Big) \\ &= \frac{1}{2}m_a^2\phi^2 + \frac{c_2}{4! c_1}\frac{m_a^2}{N^2 f_a^2}\phi^4 + \cdots. \end{aligned} \tag{3.24}$$

In this expansion, the axion mass is given by

$$\begin{aligned} m_a^2 &= \frac{1}{f_a^2 V_4}\int d^4x d^4y \left\langle \frac{g^2}{32\pi^2} G\tilde{G}(x)\, \frac{g^2}{32\pi^2} G\tilde{G}(y)\right\rangle_{\phi=0} \\ &= \left(10^{-12}\sqrt{c_1}\,\mathrm{eV}\right)^2 \left(\frac{\Lambda}{\mathrm{MeV}}\right)^4 \left(\frac{10^{15}\,\mathrm{GeV}}{f_a}\right)^2, \end{aligned} \tag{3.25}$$

where V_4 is the four-dimensional volume. The $1/N^2$ factor for the quartic term of the axion potential leads to the suppression of the anharmonic effects as long as the initial misalignment of the axion field is $\phi_i \lesssim f_a$.

The glueball and the axion can be naturally light by lowering the scale of confinement. The difference between the two is that as their masses get smaller, the glueballs interact more strongly with each other, whereas the axions interact more feebly due to the additional suppression factor $\Lambda/f_a \ll 1$. The glueball is not a lightest particle in our set-up, so it is unstable. In the lattice calculation [29, 30], the glueball mass depends on the axion field value as

$$m_g = m_g(\phi = 0)\left(1 + \mathcal{O}\Big(\frac{\phi^2}{N^2 f_a^2}\Big)\right). \tag{3.26}$$

Through the quadratic and cubic interactions of the glueball, we get the leading interaction for the decay of the glueball to two axions,

$$\frac{m_g^3}{4\pi N^3 f_a^2}\phi^2 \varphi_g. \tag{3.27}$$

From Eq. (3.27), the life-time of the glueball is estimated as $\tau_{\varphi_g} \sim 10^{17}\,\mathrm{Gyr} \times (f_a/10^{13}\,\mathrm{GeV})^4 (\mathrm{G}$ In the parameter space we will focus on, the glueball is cosmologically stable, so that both axion and glueball are dark matter of the Universe.

For cosmology, we consider the case that the dark sector and the visible sector are thermally decoupled from the beginning. Therefore, dark gluons/glueballs are thermalized by their own interactions at a temperature T_g, which is different from the photon temperature T_γ. Starting from the gluon fluid at high temperatures, as T_g

drops and crosses the dark critical temperature $T_{g,c} = \mathcal{O}(\Lambda)$, the confining phase transition occurs. Below $T_{g,c}$, all gluons are confined into the glueballs, and the evolution is described by the massive glueball fluid. The dark gluon temperature also affects the evolution of the dark axions. The leading term of the axion potential induced by the gluo-thermodynamics is

$$V(T_g, \phi) = \frac{1}{2} m_a^2(T_g) \phi^2, \tag{3.28}$$

where the axion mass $m_a(T_g)$ is well described by the dilute instanton gas approximation in the deconfining phase,

$$m_a(T_g) \simeq m_a \left(\frac{T_{g,c}}{T_g} \right)^{\eta_a} \quad \text{for} \quad T_g \gtrsim T_{g,c}, \tag{3.29}$$

with $\eta_a = 11N/6 - 2$. For $N = 3(4)$, $\eta_a = 3.5(5.3)$ [31]. After the confinement ($T_g \lesssim T_{g,c}$), the axion mass is saturated as its zero temperature value, $m_a(T_g) \simeq m_a$ [32].

Actually, the temperature dependence of the axion potential implies the existence of the energy flow from the gluon fluid to the axions as the temperature decreases. Then, a natural question is whether or not the entropy of the dark gluon also evolves during the energy transfer. In order to make it clearer, let us discuss the gluo-thermodynamics in more detail. The free energy density of the gluon/glueball fluid can be evaluated from the gluon partition function for a given temperature T_g. If the topological θ-term ($\theta \equiv \phi/f_a$) is vanishing, the free energy density f_g is only the function of the temperature as $f_g(T_g) = -p_g$, where p_g is the pressure of the gluon/glueball fluid. The energy (ρ_g) and entropy (s_g) densities are obtained by the thermodynamic relations, $s_g = -df_g/dT_g$ and $\rho_g = T_g s_g - p_g$. On the other hand, the situation is a little bit different for the non-vanishing θ-term. Because the gluon partition function also depends on θ, the free energy density (the negative of the

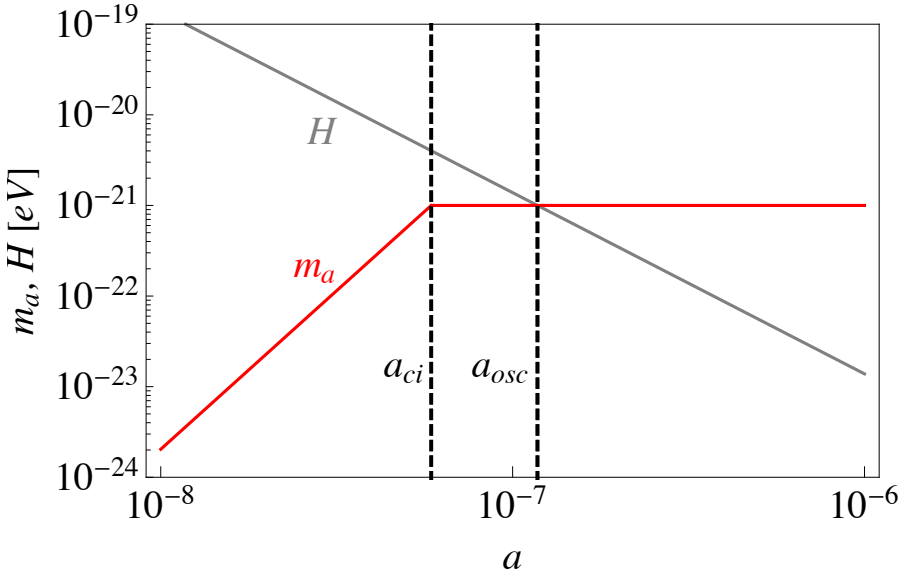

Figure 3.1 Schematic representation of the evolution of axion mass. a_{ci} is the scale factor at the confinement, and a_{osc} is the scale factor at which the axion start oscillation.

pressure for the gluon fluid with the θ-term) is evaluated as [29]

$$f_{g+\theta}(T_g) = -p_g + V(T_g, \phi), \tag{3.30}$$

where $p_g \equiv -f_g(T_g)$. The second term of the RHS represents the contribution of the vacuum energy density generated by the non-perturbative gluo-thermodynamics. The energy density of the gluon fluid with the θ-term also can be decomposed into the sum of the vacuum energy density and the pure gluonic contribution as $\rho_{g+\theta}(T_g) = \rho_g + V(T_g, \phi)$. Then, the thermodynamics relations provide

$$\begin{aligned} s_g &= -\frac{df_{g+\theta}(T_g)}{dT_g} = \frac{dp_g}{dT_g} - \frac{\partial V(T_g, \phi)}{\partial T_g} \\ &= \frac{\rho_{g+\theta}(T_g) - f_{g+\theta}(T_g)}{T_g} = \frac{\rho_g + p_g}{T_g}. \end{aligned} \tag{3.31}$$

As a result, the entropy and the energy density of the gluon/glueball fluid depend

not only on the temperature but also on the axion field value as Eq. (3.31) and

$$\rho_g = T_g \frac{dp_g}{dT_g} - p_g - T_g \frac{\partial V(T_g, \phi)}{\partial T_g}. \tag{3.32}$$

From the continuity equation of the dark sector, we can explicitly show that the entropy of the dark sector in a comoving volume $s_g a^3$ is conserved for whatever value of ϕ and its evolution except the period of the confining phase transition.

Before discussing the explicit evolution of each component, for completeness, we address general equations of motion for axion and gluon as the fluids including their homogenous and perturbation parts.

3.3.2 Dynamics of the Axion-Gluon/Gluoball Fluids

The axion dark matter is described by the evolution of the classical fields, $\phi(x)$. The dark gluon/glueball densities and their perturbations can be parameterized by its temperature evolution $T_g(x)$ and $\phi(x)$ as discussed in the previous section. In this context, $\{\phi(x), T_g(x)\}$ are good variables to derive full equations of motion of dark sector including their perturbations. Considering the fluid description, the evolution of energy densities and pressures are deduced from the evolution of ϕ and T_g with the help of the Einstein equations, gluo-thermodynamics and the lattice calculation.

In order to include perturbations, we introduce the gauge, the conformal Newtonian gauge, for the inhomogeneous part of the metric tensor

$$ds^2 = a(\tau)^2 \Big(-(1+2\Psi)d\tau^2 + (1+2\Phi)d\vec{x}^2 \Big), \tag{3.33}$$

where the conformal time τ and the conformal Hubble rate $\mathcal{H}$

$$\tau = \int \frac{dt}{a}, \quad \mathcal{H} \equiv \frac{1}{a}\frac{da}{d\tau} = \frac{a'}{a} = aH \tag{3.34}$$

are introduced. Here, $H = \dot{a}/a$ is the Hubble expansion rate for the proper time t. We use the notation

$$'\equiv \frac{d}{d\tau}, \quad \dot{} \equiv \frac{d}{dt}, \tag{3.35}$$

for the time derivatives. In Sec. 3.3 and 3.5, the conformal time is mostly taken as the argument of the time dependent variables, whereas the proper time t is used for the discussion about the late time effects of dark matter in Sec. 3.6.

Expanding ϕ and T_g near the homogeneous solutions,

$$\phi(\tau, \vec{x}) \;\; = \;\; \phi(\tau) + \delta\phi(\tau, \vec{x}) \; , \tag{3.36a}$$

$$T_g(\tau, \vec{x}) \;\; = \;\; T_g(\tau) + \delta T_g(\tau, \vec{x}) \; , \tag{3.36b}$$

the equations of motion of the background axion field is given by

$$\phi'' + 2\mathcal{H}\phi' + a^2 \frac{\partial V(T_g, \phi)}{\partial \phi} = 0. \tag{3.37}$$

The corresponding energy density and pressure are

$$\rho_a = \frac{\phi'^2}{2a^2} + V(T_g, \phi), \quad p_a = \frac{\phi'^2}{2a^2} - V(T_g, \phi). \tag{3.38}$$

From Eq. (3.37) and (3.38), the continuity equation for the background axion is obtained

$$\rho_a' + 3\mathcal{H}(1 + w_a)\rho_a = \frac{\partial V}{\partial T_g} T_g'. \tag{3.39}$$

$w_a \equiv p_a/\rho_a$ is the equation of state for the axion. Since the axion-gluon fluid is isolated from the visible sector, the total energy and pressure of dark sector should satisfy the continuity equation without source terms

$$\rho_{a+g}' + 3\mathcal{H}(\rho_{a+g} + p_{a+g}) = 0. \tag{3.40}$$

This leads to the evolution of the gluon/glueball fluid as

$$\rho_g' + 3\mathcal{H}(1+w_g)\rho_g = -\frac{\partial V}{\partial T_g}T_g', \tag{3.41}$$

where $w_g = p_g/\rho_g$. Together with Eq. (3.31), (3.32), we can derive the conservation of the dark entropy as we claimed,

$$s_g' + 3\mathcal{H}s_g = 0. \tag{3.42}$$

For the evolution of the perturbed variables, the Fourier mode of the axion field $\delta\phi$ with the wavenumber k is evolved as

$$\begin{aligned}\delta\phi'' + 2\mathcal{H}\delta\phi' + \left(k^2 + a^2\frac{\partial^2 V}{\partial\phi^2}\right)\delta\phi + \phi'(-\Psi' + 3\Phi') \\ + 2a^2\frac{\partial V}{\partial\phi}\Psi + a^2\frac{\partial^2 V}{\partial\phi\partial T_g}\delta T_g = 0.\end{aligned} \tag{3.43}$$

The axion fluid perturbation variables $\delta\rho_a$, δp_a, v_a and π_a are derived as

$$\delta\rho_a = \frac{\phi'\delta\phi' + \phi'^2\Phi}{a^2} + \frac{\partial V}{\partial\phi}\delta\phi + \frac{\partial V}{\partial T_g}\delta T_g, \tag{3.44a}$$

$$\delta p_a = \delta\rho_a - 2\frac{\partial V}{\partial\phi}\delta\phi - 2\frac{\partial V}{\partial T_g}\delta T_g, \tag{3.44b}$$

$$(\rho_a + p_a)v_a = a^{-2}k\phi'\delta\phi, \quad p_a\pi_a = 0. \tag{3.44c}$$

The definition and convention of the variables in above equations follow Ref. [33–35]. From Eq. (3.32), the gluon/glueball fluid perturbations δp_g and $\delta\rho_g$ are also related with δT_g and $\delta\phi$ as

$$\begin{aligned}\delta\rho_g &= \left(T_g^2\frac{d^2 p_g}{dT_g^2} - \frac{\partial^2 V}{\partial(\ln T_g)^2}\right)\frac{\delta T_g}{T_g} - \left(\frac{\partial^2 V}{\partial\phi\partial\ln T_g}\right)\delta\phi, \\ \delta p_g &= \frac{dp_g}{dT_g}\delta T_g.\end{aligned} \tag{3.45}$$

Similarly, from Eqs. (3.43) and (3.44), we derive the equations of motion for the

fluid perturbations.

$$\begin{aligned}
\delta_a' = \quad & -ku_a - 3(1+w_a)\Phi' \\
& -\left(3\mathcal{H} + \frac{1}{2}\frac{\partial \ln V}{\partial \ln T_g}\frac{T_g'}{T_g}\right)\left(\frac{\delta p_a}{\delta \rho_a} - w_a\right)\delta_a \\
& +\frac{1}{2}(1-w_a)\frac{d}{d\tau}\left(\frac{\partial \ln V}{\partial \ln T_g}\frac{\delta T_g}{T_g}\right), \qquad (3.46a) \\
u_a' = \quad & -\mathcal{H}(1-3w_a)u_a + k(1+w_a)\Psi + k\frac{\delta p_a}{\delta \rho_a}\delta_a \\
& -\frac{1}{2}(1-w_a)\frac{\partial \ln V}{\partial \ln T_g}\left(\frac{T_g'}{T_g}u_a - k\frac{\delta T_g}{T_g}\right), \qquad (3.46b) \\
\delta_g' = \quad & -ku_g - 3(1+w_g)\Phi' - 3\mathcal{H}\left(\frac{\delta p_g}{\delta \rho_g} - w_g\right)\delta_g \\
& +\frac{1}{2}\frac{\rho_a}{\rho_g}\left[\frac{\partial \ln V}{\partial \ln T_g}\frac{T_g'}{T_g}\left\{\left(\frac{\delta p_a}{\delta \rho_a} - 1\right)\delta_a + (1-w_a)\delta_g\right\}\right. \\
& \qquad \left. -(1-w_a)\frac{d}{d\tau}\left(\frac{\partial \ln V}{\partial \ln T_g}\frac{\delta T_g}{T_g}\right)\right], \qquad (3.46c) \\
u_g' = \quad & -\mathcal{H}(1-3w_g)u_g + (1+w_g)k\Psi + k\frac{\delta p_g}{\delta \rho_g}\delta_g \\
& +\frac{1}{2}(1-w_a)\frac{\partial \ln V}{\partial \ln T_g}\left(\frac{T_g'}{T_g}u_g - k\frac{\delta T_g}{T_g}\right), \qquad (3.46d)
\end{aligned}$$

where $\delta_a = \delta\rho_a/\rho_a$, $u_a = (1+w_a)v_a$, and same definitions for δ_g, u_g. Note that $\{\delta p_a, \delta p_g, \delta T_g, \delta\phi\}$ can be expressed by $\{\delta_a, \delta_g, u_a\}$ using Eq. (3.44) and (3.45), and solve the equations of $\{\delta_a, \delta_g, u_a, u_g\}$. Otherwise, the full equations also can be expressed by $\{\delta\phi, \delta T_g, u_g\}$. Compared with the isolated axion and gluon/glueball perturbations, the equations contain the terms proportional to $\partial V/\partial T_g$, which originate from the non-perturbative interactions between the gluon and the axion. With the T_g dependent axion potential given by Eq. (3.29), the contribution of these terms becomes larger as T_g approaches to $T_{g,c}$.

The amount of dark gluons can be parameterized by the ratio between the entropies of the dark sector and the visible sector, s_g/s_{SM}. Although dealing with the entropy ratio between two sectors would be easier to trace the evolution of the densi-

ties, in order to have a more intuitive picture about how cold the gluons are compared to the SM sector, we will use the ratio parameter between the temperatures. Taking a period around the phase transition, the photon temperature when T_g arrives at $T_{g,c}$ is denoted by $T_{\gamma,c}$. Then, we define the ratio parameter r as

$$r \equiv \left(\frac{g_{*S}(T_{\gamma,c})}{2(N^2-1)} \frac{s_g}{s_{SM}} \right)^{1/3} \simeq \frac{T_{g,c}}{T_{\gamma,c}}, \tag{3.47}$$

where s_g ($s_{\rm SM}$) is the entropy density of the gluon fluid (the SM sector), and g_{*S} is the effective number of degrees of freedom in entropy for the SM sector.

Up to now, we have ignored the effect of dissipation induced by the background dark gluon plasma. Although, it is not crucial in our discussion, let us clarify the condition that our assumption is invalid. Including the friction term ($\gamma_{\rm fr}$) for the axion's motion, the equation of motion of the background axion is written as [36]

$$\ddot{\phi} + (3H + \gamma_{\rm fr})\,\dot{\phi} + m_a^2(T_g)\phi = 0. \tag{3.48}$$

In the deconfining phase, $\gamma_{\rm fr} = \Gamma_{\rm sph}(T_g)/f_a^2 T_g$, where the sphaleron rate is estimated as [37]

$$\begin{aligned} \Gamma_{\rm sph}(T_g) &= \int d^4x \left\langle \frac{g^2}{32\pi^2} G\tilde{G}(x)\, \frac{g^2}{32\pi^2} G\tilde{G}(0) \right\rangle_{T_g} \\ &= \mathcal{O}(0.1-1) \left(\frac{g^2 N}{4\pi} \right)^5 \left(\frac{N^2-1}{N} \right) T_g^4, \end{aligned} \tag{3.49}$$

for $g^2/4\pi \lesssim 0.1$. Around the critical temperature, $T_g \sim T_{g,c}$ the gauge coupling can be as large as $g^2N/4\pi = \mathcal{O}(1)$. In this regime, the sphaleron rate is expected as $\Gamma_{\rm sph}(T_{g,c}) \sim T_{g,c}^4$ from the dimensional analysis. After the confining phase transition, no reliable calculation has been done so far. A crude estimation based on the dimensional analysis is that the dissipation rate is at most proportional to the entropy density (or number density) of the glueballs as $\gamma_{\rm fr} \sim s_g/f_a^2$. Because the time dependence of the Hubble rate and the dissipation rate are given as $H \propto a^{-2}(a^{-3/2})$ in

radiation dominated era (matter dominated era) and $\gamma_{\rm fr} \propto a^{-3}$, the gluon induced friction term is important only when the temperature of the visible sector becomes greater than

$$T_\gamma > \mathcal{O}(1) \left(\frac{10^9\,\mathrm{GeV}}{Nr^3}\right) \left(\frac{10^{14}\,\mathrm{GeV}}{f_a}\right)^2 \left(\frac{g^2 N}{4\pi}\right)^{-5}. \tag{3.50}$$

Comparing this with the temperature when the axion starts to oscillate ($T_\gamma < \mathrm{TeV}$), it is always irrelevant.

3.4 Evolution History

3.4.1 Evolution of the Background Gluon and Glueballs

In Eqs. (3.39-3.46), we establish the continuity equations for the background and perturbative variables based on the equations of motion of the axion field, and gluo-thermodynamics. On one hand, the dependence on the temperature of ρ_g and p_g should be clarified. It is particularly easy for $T_g \gg T_{g,c}$ and $T_g \ll T_{g,c}$. In the limit of $T_g \gg T_{g,c}$, gluons are just relativistic fluid. Therefore,

$$\begin{aligned} p_g &= \frac{\pi^2}{45}(N^2-1)\,T_g^4, \\ \rho_g &= \frac{\pi^2}{15}(N^2-1)\,T_g^4 = 3p_g. \end{aligned} \tag{3.51}$$

and the axion-gluon interaction is negligible because

$$-\frac{\rho_a}{\rho_g}\frac{\partial \ln V}{\partial \ln T_g} = \frac{2\eta_a \rho_a}{\rho_g} \lesssim \frac{0.7 c_1 \eta_a}{(N^2-1)} \left(\frac{T_{g,c}}{T_g}\right)^{2\eta_a+4}. \tag{3.52}$$

However, as the gluon temperature approaches $T_{g,c}$, Eq. (3.51) does not hold. The true dependence on the gluon temperature can only be figured out by the lattice

calculation [38–40]. We adopt the lattice data with $\theta = 0$, and deduce the densities for nonzero θ case based on the data of gluon/glueball pressure $p_g(T_g)$.

At $T_{g,c}$, the dark gluons are combined into dark glueballs with masses of multiples of the confining scale Λ [41–44]. Here, Λ is defined with a certain regularization scheme. Taking the $\overline{MS}$ scheme, the lattice results with the functional method [45,46] show that

$$\frac{T_{g,c}}{\Lambda} \simeq 1.2 + \frac{0.27}{N^2}. \tag{3.53}$$

The phase transition is first-order if $N > 2$. In order to understand how long the phase transition happens, we compare the energy density in the deconfined phase with that of the confined phase at $T_{g,c}$. The former is the energy density of the gluon fluid of $\mathcal{O}(0.1N^2T_{g,c}^4)$, and the latter is the sum of the tower of the glueballs of $\mathcal{O}(0.1T_{g,c}^4)$. Thus, as N increases, larger latent heat is released and the transition period becomes longer. Let us shortly discuss how we evaluate the energy density of the glueballs.

Since the lightest glueball mass is calculated as [42, 47]

$$\frac{m_g}{T_{g,c}} = (5-6)\Big(1 + \mathcal{O}(1/N^2)\Big), \tag{3.54}$$

all glueballs are non-relativistic at $T_{g,c}$. With the help of the spectral density $\hat{\rho}(m)$, the energy density of glueballs can be written as

$$\rho_g(T_{g,c}) = \int_0^\infty dm\, \hat{\rho}(m)\, m \left(\frac{mT_{g,c}}{2\pi}\right)^{3/2} e^{-m/T}. \tag{3.55}$$

$\hat{\rho}(m)$ is approximated by the sum of the discrete low-lying resonances with masses $m_g(J^{PC})$, where J (angular momentum), P (parity), and C (charge conjuration) are the eigenvalues of the states, and the continuum spectrum of the Hagedorn tower

$$\begin{aligned}\hat{\rho}(m) \;\simeq\; & \sum_{m<m_{\rm th}} (2J+1)\delta\left(m - m_g(J^{PC})\right) \\ & + \frac{n_N}{m}\Big(\frac{2\pi T_H}{3\,m}\Big)^3 e^{m/T_H}\Theta(m - m_{\rm th}),\end{aligned} \tag{3.56}$$

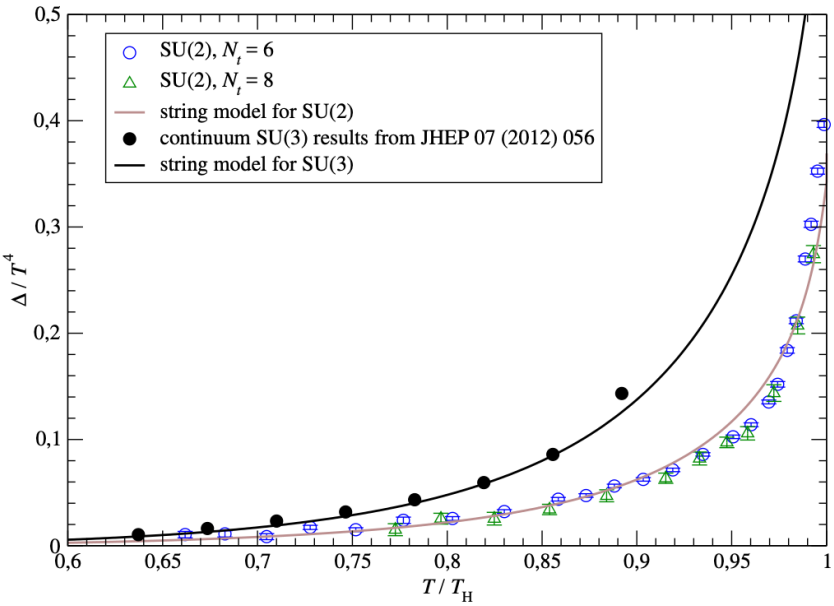

Figure 3.2 Comparison of trace anomaly between the result from lattice calculation and from analytic formula based on the spectral density in Eq. (3.56), from Ref. [48].

where $n_2 = 1$, $n_{N\geq 3} = 2$, and the threshold mass $m_{\rm th}$ is usually chosen as $2m_g$. The Hagedorn temperature T_H is related with $T_{g,c}$ as [48]

$$\frac{T_H}{T_{g,c}} \simeq 1.16 - \frac{0.8}{N^2}. \tag{3.57}$$

Note that even if N increases, the number of degrees of freedom of the glueballs does not increase. Therefore, the contribution from the Hagedorn glueballs is insensitive to N and becomes $\mathcal{O}(0.01-0.1)T_{g,c}^4$. The low-lying glueball contributions are $\mathcal{O}(10-50)\%$ of it. We adopt the spectrum of the glueballs in Ref. [42].

The lower limit of the actual transition period is given by the period assuming the quasi-equilibrium transition, i.e. the pressures of deconfining/confining phases are equal and the latent heat is released adiabatically as the Universe expands. In this case, the temperatures of the confining and deconfining phases are the same and

maintained at around $T_{g,c}$. The duration of the phase transition is estimated by the conservation of the dark entropy:

$$a_{cf} = a_{ci} \left(\frac{s_{\rm gluon}(T_{g,c})}{s_{\rm glueball}(T_{g,c})} \right)^{1/3} \simeq a_{ci} N^{2/3}, \tag{3.58}$$

where a_{cf} (a_{ci}) is the scale factor when the phase transition ends (starts), $s_{\rm gluon}(T_{g,c})$ ($s_{\rm glueball}(T_{g,c})$) denotes the entropy density of the dark gluon (glueball) at $T_g = T_{g,c}$. The N-dependence of the duration is obtained from $s_{\rm gluon}(T_{g,c}) \simeq 0.1 N^2 T_{g,c}^2 \simeq N^2 s_{\rm glueball}(T_{g,c})$.

The phase transition becomes stronger first-order as N increases. Thus, the additional entropy is generated during the transition and makes the glueballs hotter than the previous estimation. However, this effect is negligible unless $N \gg 4\pi$, because the nucleation temperature is just around $T_{g,c}$ and the strong interactions of the gluon and glueball fluids provide a large friction coefficient for the bubble wall propagation. For $N = 3$, $a_{cf} \simeq 2 a_{ci}$ is obtained numerically, which is well matched with our parametric estimation $N^{2/3}$. The assumption of dark entropy conservation will be kept in the following discussion.

After the transition, the Hagedorn contribution becomes negligible as the scale factor increases by an order of magnitude compared to a_{cf}. The contribution of the low-lying glueballs maintains chemical equilibrium by two-to-two and three-to-two scatterings whose rates are estimated as

$$\sigma_{2\to 2} v \sim \frac{v_f (4\pi/N)^4}{32\pi m_g^2}, \quad \sigma_{3\to 2} v^2 \sim \frac{(4\pi/N)^6}{(4\pi)^3 m_g^5}, \tag{3.59}$$

where v_f is the relative velocity of the final particles from the scattering. The detailed description of the evolution of low-lying stable glueballs is provided in [49]. If the P and T violating topological θ-term is absent, these glueballs can be classified as the eigenstates of J^{PC}. In our set-up, because of the axion's motion, the time dependent mixings can arise between different P eigenstates, *e.g.* between 0^{++} and 0^{-+}. As a

result, the terms like

$$\Delta\mathcal{L} \sim m_g \frac{\phi}{f_a} \varphi_{++}^2 \varphi_{-+} \tag{3.60}$$

may be generated. It turns out that theses mixings do not lead to the decay of heavier state to the light states by the kinematic reason. We expect that the stability of low lying glueballs is not altered by the axion's evolution.

As the universe expands, the $3 \to 2$ process freezes out when the most of the $2 \to 2$ processes still active. This is because the interaction rate of the $3 \to 2$ process is proportional to the square of the number density of the glueballs, while that of the $2 \to 2$ processes is linearly proportional to the number density of the glueballs. Therefore, the relative chemical equilibrium holds between different glueball states. Since the $3 \to 2$ process of the lightest glueball keeps the chemical potential of the lightest glueball to be zero, the chemical potential of all glueball states is zero until the $3 \to 2$ process of the lightest glueball freezes out. Before the freeze-out of $3 \to 2$ interactions, a single glueball state with a mass m_g in thermal equilibrium is given by

$$\begin{aligned} \rho_g(T_g) &= m_g \left(\frac{m_g T_g}{2\pi}\right)^{3/2} e^{-\frac{m_g}{T_g}} \left(1 + \frac{27}{8}\frac{T_g}{m_g} + \mathcal{O}\left(\frac{T_g^2}{m_g^2}\right)\right), \\ p_g(T_g) &= T_g \left(\frac{m_g T_g}{2\pi}\right)^{3/2} e^{-\frac{m_g}{T_g}} \left(1 + \frac{15}{8}\frac{T_g}{m_g} + \mathcal{O}\left(\frac{T_g^2}{m_g^2}\right)\right). \end{aligned} \tag{3.61}$$

The total energy density and pressure of the glueballs can be obtained by summing Eq. (3.61) over all low-lying stable glueballs. It is found that the contributions other than the lightest glueball become negligible for $T_g \lesssim 0.5 T_{g,c}$.

A distinguishing properties of the dark matter with the three-to-two self-interaction is the scaling behavior as the Universe expands. The temperature of the glueballs drops much slower than that of the photon during its chemical equilibrium maintain-

ing $s_g \propto 1/a^3$, so $T_g \sim 1/\ln a$. The energy density

$$\rho_g \simeq T_g s_g \propto \frac{1}{a^3 \ln a}, \tag{3.62}$$

drops faster than that of a cold dark matter, since the three-to-two self-interaction converts the mass energy to the kinetic energy. This behavior ends when the process freezes out at $T_g = T_{g,fo}$ with

$$\rho_g^2(T_{g,fo}) \simeq \frac{(3m_g T_{g,fo})(H|_{T_g=T_{g,fo}})}{\langle \sigma_{3\to 2} v^2 \rangle}. \tag{3.63}$$

After that, the glueballs act as free-streaming particles. Using Eq. (3.63) and the dark entropy conservation, the freeze-out temperature is evaluated as

$$\begin{aligned} &\frac{m_g}{T_{g,fo}} + \frac{5}{4}\ln\frac{m_g}{T_{g,fo}} + \frac{3}{4}\ln\frac{m_g}{\mathrm{MeV}} \\ &\simeq 28.2 + \frac{3}{2}\ln\frac{r}{0.01} - \frac{7}{2}\ln\frac{N}{3}, \end{aligned} \tag{3.64}$$

if it happens during radiation dominated era. As a specific example, for $N = 3$, $r = 0.01$, and $m_g = 1\,\mathrm{MeV}$, we get

$$T_{g,fo} \simeq 0.04\, m_g \simeq 0.2\, T_{g,c}. \tag{3.65}$$

The relation $T_{g,fo} = \mathcal{O}(0.2) T_{g,c}$ is not much sensitive to the values of r and m_g that we are interested in.

During the evolution of the glueballs, the photon temperature also evolves. When the dark glueballs freeze-out, the photon temperature becomes

$$T_{\gamma,fo} \simeq 3\,\mathrm{keV} \left(\frac{N}{3}\right)^{1/2} \left(\frac{0.01}{r}\right)^{3/2} \left(\frac{m_g}{\mathrm{MeV}}\right)^{5/4}. \tag{3.66}$$

We can also easily evaluate the case that the freeze-out of the dark glueball happens after the matter-radiation equality for $m_g < \mathrm{keV}$.

So far, we have specified all history of the gluons and glueballs in order to identify the time dependence of the glueball temperature $T_g(\tau)$ for Eq. (3.46). For the final

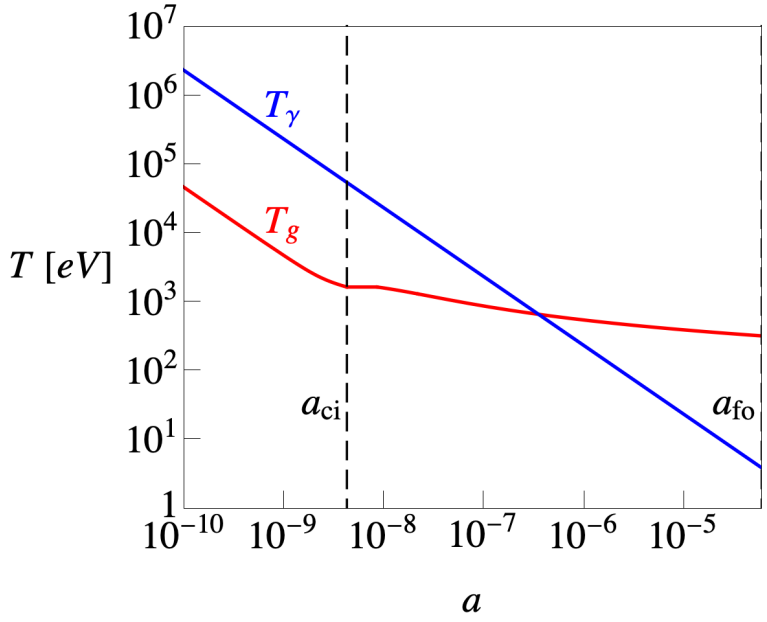

Figure 3.3 Schematic plot for the evolution of the gluon (glueball) temperature and the photon temperature. While the photon temperature T_γ drops proportional to a^{-1}, T_g is a constant during the first order phase transition and then proportional to $1/\ln a$ during the glueball phase.

relic density of the glueballs, it can be evaluated in a much simpler way from the conservation of the entropy of dark sector as

$$\begin{aligned}\Omega_g h^2 &\simeq 0.014 \left(\frac{N^2-1}{10}\right)\left(\frac{r}{0.01}\right)^3\left(\frac{T_{g,fo}}{10\,\mathrm{keV}}\right)\left(\frac{3.94}{g_{*S}(T_{\gamma,c})}\right)\\ &\simeq 0.014 \left(\frac{N^2-1}{10}\right)\left(\frac{r}{0.01}\right)^4\left(\frac{T_{\gamma,c}}{5\,\mathrm{MeV}}\right)\left(\frac{3.94}{g_{*S}(T_{\gamma,c})}\right)\\ &\simeq 0.12 \left(\frac{N^2-1}{10}\right)\left(\frac{r}{0.003}\right)^3\left(\frac{m_g}{100\,\mathrm{MeV}}\right)\left(\frac{3.94}{g_{*S}(T_{\gamma,c})}\right).\end{aligned} \tag{3.67}$$

3.4.2 Evolution of the Background Axion

The lattice studies provide the coefficient of each term in perturbation expansion of the axion scalar potential Eq. (3.24) as [50].

$$c_1 \simeq 0.3 + \frac{1}{N^2}, \quad c_2 \simeq -2.7 c_1. \tag{3.68}$$

One interesting feature of the axion potential is that it is not a single branch, but multiple (N) branches, where for each branch the period of the scalar potential is $2\pi N f_a$ [51]. The general expression of the scalar potential for a kth branch is

$$V_k = N^2 \Lambda^4 h\left(\frac{\phi}{N f_a} + \frac{2\pi k}{N}\right) \quad k = 1, \cdots, N, \tag{3.69}$$

where $h(\psi)$ is the 2π-periodic function. At present, calculation of the full shape of the potential is not available. Besides the lattice study, the scalar potential for the part of axion field range was studied in the large N limit using the holographic description of the pure $SU(N)$ gauge theory [52, 53]. The 't Hooft coupling $\lambda = g^2 N$ at the KK scale in the dual gravity theory can be matched with that deduced from the axion potentials of the lattice calculation Eq. (3.68). We find that $\lambda = 10 - 20$ gives a reasonable matching.

At high temperatures of the gluons, the instanton approximation for the axion potential is valid, and there is a single branch. During the phase transition, branches will emerge, and the axion can be located in a different branch in a different patch of the Universe. If each branch provides a stable axion trajectory, we have to consider the effect of them seriously.

Following the approach of the holographic description as in [52], we estimate the tunneling rate between kth to $k-1$th branches.

$$\Gamma_{\text{tunneling}} \propto e^{-S_{(k \to k-1)}}, \tag{3.70}$$

where the Euclidean action is

$$S_{(k\to k-1)} = \mathcal{O}(10^{-11})N\frac{(N/k)^3}{(1+\frac{\mathcal{O}(1)k^2}{N^2})^2}. \tag{3.71}$$

This can be significantly large only when $N \gtrsim 10^3$. Therefore, in our consideration, all branches with higher energy densities are quite unstable, and the transition to the lowest energy state will occur almost immediately. As a result, the effective potential of the axion is well described by

$$V(\phi) = \min_k V_k(\phi), \tag{3.72}$$

and one can think the evolution of the axion within the range $2\pi f_a$.

Without worrying about the effect of other branches, Eq. (3.37) gives

$$\phi'' + 2\mathcal{H}\phi' + a^2 m_a^2(T_g)\phi = 0, \tag{3.73}$$

for $\phi \lesssim f_a$. If the second term of the LHS is much larger than the third term, the axion field is approximately constant because of the large Hubble friction. This is the slow-roll limit. In the opposite case, the axion field oscillates with the oscillation frequency $m_a(T_g)$. Such evolution can be well approximated by the simple transition at $a = a_{osc}$ to satisfy $3\mathcal{H} = am_a(T_g)$ ($3H = m_a(T_g)$). For each epoch,

$$\begin{aligned} \phi(\tau) &\simeq \phi_i \equiv f_a\theta_i \quad (a < a_{osc}) \\ &\simeq \mathcal{A}(\tau)\cos\Big(\int^\tau d\tilde{\tau}a(\tilde{\tau})m_a(T_g(\tilde{\tau}))\Big), \quad (a > a_{osc}) \end{aligned} \tag{3.74}$$

where θ_i is the initial misalignment angle of the axion field, $\mathcal{A}(\tau)$ is slowly varying function with $\mathcal{A}'/\mathcal{A} \ll am_a(T_g)$. The axion acts like dark energy during $a < a_{osc}$, while for $a > a_{osc}$, the axion plays the role of cold dark matter because $\langle w_a\rangle \simeq 0$ by averaging out the fast oscillation. The initial axion value ϕ_i is not deterministic. Since both $\theta_i \ll 1$, and $|\theta_i - \pi| \ll 1$ need some tuning or special model building, here we take

$$\theta_i = \mathcal{O}(1). \tag{3.75}$$

Since the axion's mass depends on the history of the dark gluons (Eq. (3.29)), there are two characteristic scales which determine the evolution history of the axion: a_{osc} (onset of the axion oscillation) and a_{ci} (onset of the confining phase transition). As the scale factor approaches a_{ci}, the contribution of the gluons to the axion's potential becomes substantial, and the axion mass is saturated. The evolution of the axion mass is smooth unless N is very large. There is no significant distinction between the deconfined and confined phases.

With the help of the lattice data, we find that the following quantity

$$R(r, f_a) \equiv \Big(\frac{r}{0.01}\Big)^2 \Big(\frac{6 \times 10^{13}\,\mathrm{GeV}}{f_a}\Big) \tag{3.76}$$

determines whether or not the axion starts to oscillate before the confining transition. If $R(r, f_a) > 1$, the axion starts to oscillate before the phase transition. The corresponding photon temperature becomes

$$T_{\gamma,osc} \simeq R(r, f_a)^{\frac{1}{2+\eta_a}} T_{\gamma,c}. \tag{3.77}$$

Otherwise ($R(r, f_a) < 1$), the axion oscillation happens after the phase transition when T_γ becomes

$$T_{\gamma,osc} \simeq R(r, f_a)^{\frac{1}{2}} T_{\gamma,c}. \tag{3.78}$$

For the evolution of the axion density, the initial density of the axion at $T_\gamma = T_{\gamma,osc}$ is approximated as

$$\rho_a \simeq \frac{1}{2} m_a^2(T_{g,osc}) f_a^2 \theta_i^2. \tag{3.79}$$

After that, the axion field will oscillate with the time dependent frequency. For the combination

$$N_a = \frac{a^3 \rho_a}{m_a(T_g)}, \tag{3.80}$$

Eq. (3.39) gives

$$N_a' + \left(3\mathcal{H} + \frac{m_a'(T_g(\tau))}{m_a(T_g(\tau))}\right) w_a N_a = 0. \tag{3.81}$$

Since the fast oscillation of the axion field means $\langle w_a \rangle = 0$, $N_a' \simeq 0$ and N_a is nearly conserved, i.e. $\rho_a/m_a(T_g) \propto 1/a^3$. Therefore, if $R(r, f_a) > 1$, the axion starts to oscillate before the confining phase transition ($T_{\gamma,osc} > T_{\gamma,c}$), and the present relic density of the axion dark matter becomes

$$\Omega_a h^2 \simeq 0.8 \times 10^{-3} \theta_i^2 \left(\frac{r}{0.01}\right)^4 \left(\frac{T_{\gamma,c}}{5\,\mathrm{MeV}}\right) R(r, f_a)^{-\frac{3+\eta_a}{2+\eta_a}}. \tag{3.82}$$

If $R(r, f_a) < 1$, the axion oscillates after the confining phase transition ($T_{\gamma,osc} < T_{\gamma,c}$). The corresponding axion dark matter density is given by

$$\begin{aligned} \Omega_a h^2 &\simeq 0.8 \times 10^{-3} \theta_i^2 \left(\frac{r}{0.01}\right)^4 \left(\frac{T_{\gamma,c}}{5\,\mathrm{MeV}}\right) R(r, f_a)^{-\frac{3}{2}} \\ &\simeq 0.05 \theta_i^2 \left(\frac{r}{0.01}\right) \left(\frac{T_{\gamma,c}}{5\,\mathrm{MeV}}\right) \left(\frac{f_a}{10^{15}\,\mathrm{GeV}}\right)^{3/2} \\ &\simeq 0.15 \left(\frac{m_a}{10^{-22}\,\mathrm{eV}}\right)^{1/2} \left(\frac{f_a}{10^{17}\,\mathrm{GeV}}\right)^2. \end{aligned} \tag{3.83}$$

As shown in Eq. (3.82), the glueballs dominate the total energy density of dark matter if the axion oscillation happens earlier than the confining phase transition. The reason is simply that initial axion energy density before the oscillation is bounded by the confining scale Λ^4. On on hand, if r^2/f_a becomes small enough, so that the axion starts to oscillate after the phase transition, the axion becomes a dominant component of dark matter.

Fig. 3.4 and Fig. 3.4 shows the evolution of dark matter densities for both glueball and axion domination scenarios. Fig. 3.6 shows the parametric dependence of the current relic abundance of the dark matter. The axes are represented by $T_{\gamma,c}$, the photon temperature when the confining phase transition of the dark gauge sector

starts, and m_a, the zero temperature axion mass, defined in Eq. (3.25) with Eq. (3.68), respectively. As we discussed, the dark matter today is dominated by the axion in the region $T_{\gamma,osc} < T_{\gamma,c}$. The glueballs are dominant dark matter today in the region $T_{\gamma,c} < T_{\gamma,osc}$.

There are various astrophysical observations to constraint the mass of the glueball and axion dark matter. We shortly summarize the bounds on it. When the glueball dominates dark matter, its self-interaction gives observable effects if the scattering rate is large enough to reach the isothermal density profile inside the halo. It can be also detectable from the merger of dark matter halos, because the glueballs will be slowed down during the collision, which leads to the offset between the dark matter and the collisionless components like stars. The cross-section of the glueball like self-interacting dark matter is bounded as ([54] and references therein)

$$\begin{aligned} \frac{\sigma_{2\to 2}}{m_g} &\simeq \left(\frac{4}{N}\right)^4 \frac{1}{m_g^3} \simeq \left(\frac{4}{N}\right)^4 \left(\frac{m_g}{60\mathrm{MeV}}\right)^{-3} \mathrm{cm}^2/\mathrm{g} \\ &\lesssim \mathcal{O}(0.5-5)\,\mathrm{cm}^2/\mathrm{g}. \end{aligned} \tag{3.84}$$

In terms of the glueball mass, the glueball should have the mass greater than $\mathcal{O}(50)$MeV if it is the dominant component of dark matter. The phenomenology of heavier glueball dark matter was studied in [55].

If the axion is the dominant dark matter component, there is also the lower bound on the axion mass due to its fuzziness. The de Broglie wavelength becomes astrophysical scale if m_a is around $10^{-22}\,\mathrm{eV}$, and suppresses the structure formation. The ultra-light axion dark matter can act like waves that are bound to or interact with each other by gravity inside the halo, which leads to the formation of solitonic cores and macroscopic quasiparticles moving around the center. These structures can have a great influence on the motion of stars. All these considerations give the strong constraint on the axion mass in the range $m_a \lesssim 10^{-22} - 10^{-20}\mathrm{eV}$ ([56,57] and references therein). There is another constraint due to the observation of highly spinning black

holes, even if the axion is not dark matter. That is because if the axion mass is close to the inverse of the size of the spinning black hole, a superradiance phenomenon occurs and parts of black hole's mass and spin are removed by the produced axion cloud. Current observations of the supermassive black hole with the mass of $10^6 - 10^7\, M_\odot$ provide interesting constraints within the axion mass range $10^{-20} - 10^{-16}\,\mathrm{eV}$ ([58] and reference therein). However, it is sensitive to the axion self-interaction, the constraint is model dependent.

When the dark matter is mostly composed of the axions, $\Omega_a h^2 \simeq 0.11$, and the freeze-out of the glueball happens after the BBN, the fraction of the dark glueball subcomponent dark matter becomes

$$\begin{aligned} f_g &\equiv \frac{\Omega_g}{\Omega_{\rm DM}} \simeq 0.28 \left(\frac{N^2-1}{10\,\theta_i^2}\right) \left(\frac{r}{0.01}\right)^3 \left(\frac{10^{15}\,\mathrm{GeV}}{f_a}\right)^{3/2} \\ &\simeq 0.02 \left(\frac{N^2-1}{10}\right) \left(\frac{r}{0.01}\right)^3 \left(\frac{m_g}{0.05\,\mathrm{MeV}}\right). \end{aligned} \tag{3.85}$$

One can think that there is no strong constraint on the subcomponent glueball dark matter for $f_g \lesssim 0.1$. However, the evolution of the glueball dark matter after structures form may alter the cosmological history of the Universe around $z = 7-15$ as discussed in Sec. 3.6.

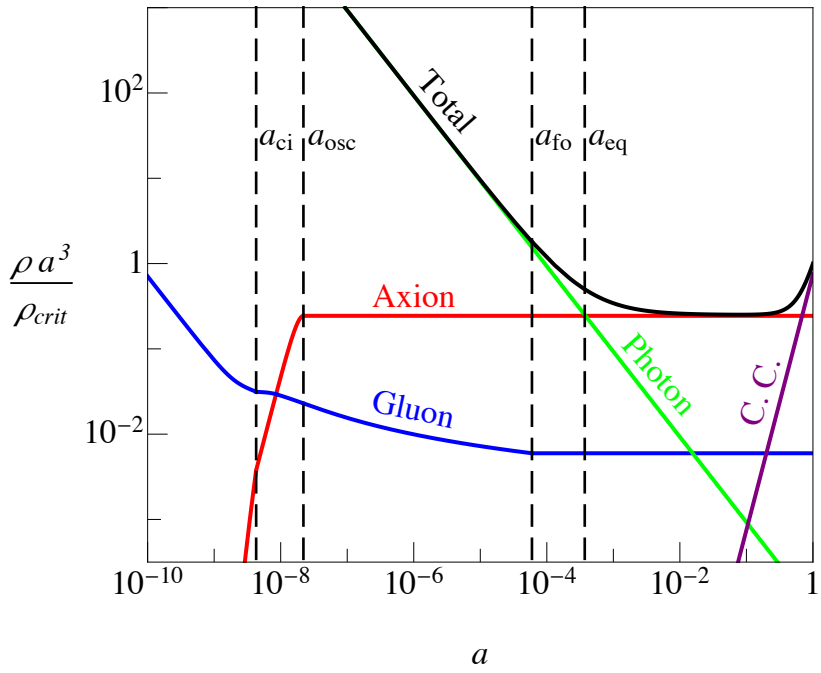

Figure 3.4 An example of the evolution of the energy density for the case of the axion-dominated. After the confinement, the number-changing self-interaction of the glueballs reduces its total number only logarithmically. The energy density of the axion is $\mathcal{O}\left(\rho_g/N^2\right)$ at the time of confinement and dominates that of the glueballs afterward.

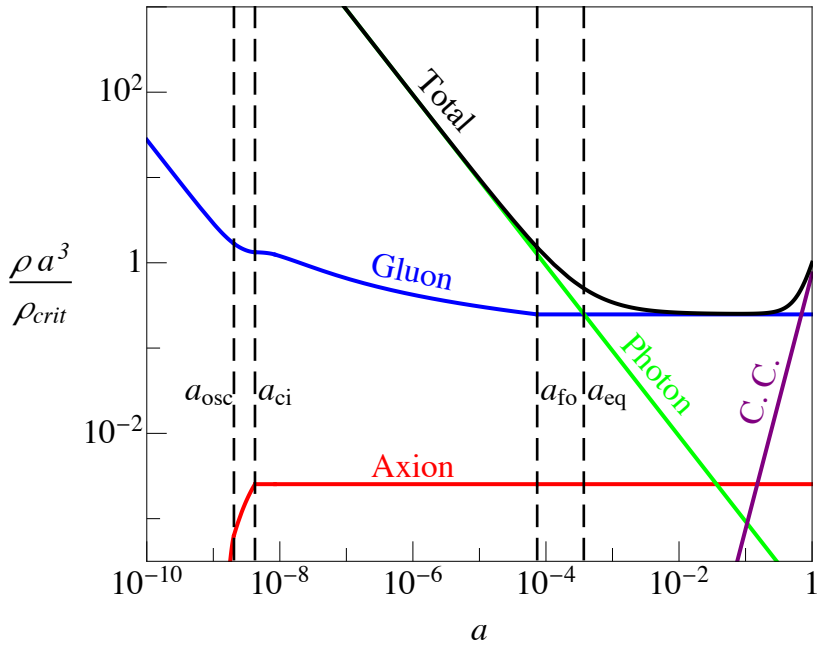

Figure 3.5 An example of the evolution of the energy density for the case of the glueball-dominated (right). The energy density of the gluon and the glueballs is much larger than that of the axion for all epoch.

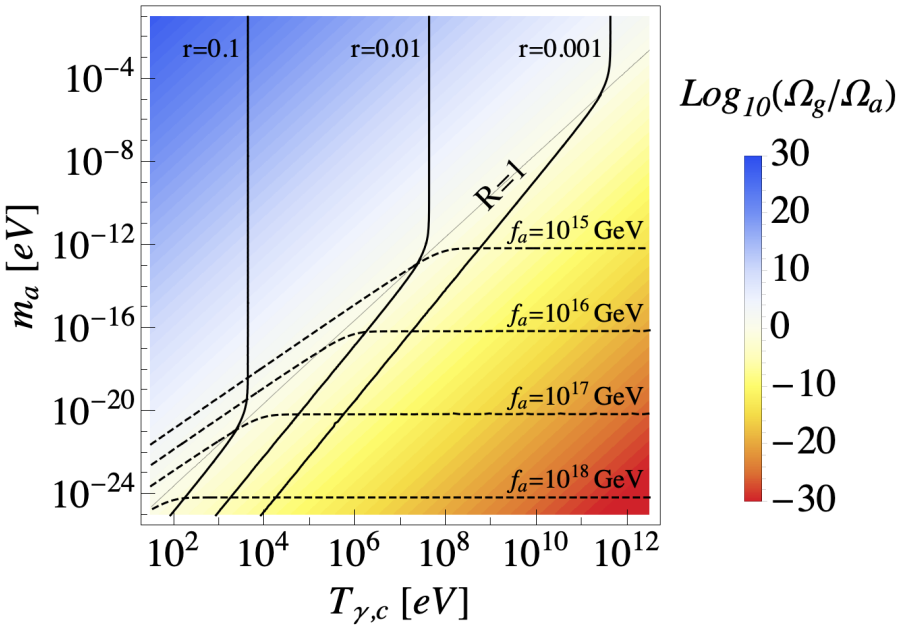

Figure 3.6 Parametric dependence of the relic abundance of the glueball and the axion for $\Omega_{\rm DM}h^2 = 0.11$. m_a is the zero-temperature axion mass and $T_{\gamma,c} \simeq T_{g,c}/r$ is the photon temperature when the confining phase transition of the dark sector starts. For the region above the line $R(r, f_a) = 1$, the oscillation of the axion starts earlier than the confinement phase transition and the gluebll is the dominant dark matter component with the mass $m_g \simeq 6\, r T_{\gamma,c}$, while below $R(r, f_a) = 1$, the axion starts to oscillate after the transition. Here, we did not impose the constraints from the current bound, which are discussed in text.

3.5 Perturbations

We now study the evolution of the cosmological perturbations for the axion and glueball dark matter. Both have non-trivial features compared to the CDM. For example, the transition of the nature of the axion from dark energy to dark matter modifies the early ISW effect of the cosmic microwave background [59]. The perturbation at scales smaller than the effective de Broglie wavelength is suppressed by its wave nature [60–62]. For glueballs, the number-changing self-interaction also disturbs the growth of the density perturbation of the scales which enter the horizon well before the freeze-out [63, 64].

On one hand, in our set-up, the dark sector is decoupled from the visible sector and the origin of their abundance can be totally different from that of the SM particles. Let us provide a simple example for it. As the origin of Eq. (3.22), the axion can originate from the phase of a complex scalar field X. The corresponding matter Lagrangian at high scales is

$$\begin{aligned} -\frac{\mathcal{L}_M}{\sqrt{-g}} &= |\partial_\mu X|^2 + \bar{Q} i\gamma^\mu D_\mu Q + \frac{\lambda}{4}\Big(|X|^2 - \frac{f_a^2}{2}\Big)^2 \\ &\quad + y X\, \bar{Q} P_L Q + h.c.. \end{aligned} \tag{3.86}$$

Here Q is the vector-like fermion charged under the dark gauge group. We have the anomalous global symmetry:

$$U(1)_{\rm PQ}:\ X \to e^{-2i\alpha} X,\ Q \to e^{-i\gamma_5 \alpha} Q. \tag{3.87}$$

After X gets a nonzero vacuum expectation value from the scalar potential, it can be decomposed as

$$X(x) = \frac{f_a + s(x)}{\sqrt{2}} e^{-i\phi(x)/f_a}. \tag{3.88}$$

The axion ϕ is massless at perturbative level, and the radial scalar s gets a mass as $m_s = \sqrt{\lambda/2} f_a$, which can be much smaller than f_a for $\lambda \ll 1$. The mass of dark

fermion is $M_Q = y f_a/\sqrt{2}$. At scales $\mu < M_Q$, integrating out the heavy fermion yields the following Lagrangian

$$\begin{aligned} -\frac{\mathcal{L}_{M\text{eff}}}{\sqrt{-g}} &\simeq \frac{1}{2}(\partial_\mu s)^2 + \frac{1}{2}m_s^2 s^2 + \frac{1}{4}\left(1 + \frac{g^2 s}{8\pi^2 f_a}\right)(G^a_{\mu\nu})^2 \\ &\quad + \frac{1}{2}\left(1 + \frac{2s}{f_a}\right)(\partial_\mu \phi)^2 + \frac{g^2 \phi}{32\pi^2 f_a} G^a_{\mu\nu}\tilde{G}^{a\mu\nu}. \end{aligned} \tag{3.89}$$

The interaction between s (ϕ) and dark gluons is coming from the one-loop diagram mediated by the heavy fermion Q. Finally the radial scalar s is decoupled at scales $\mu \ll m_s$, and we arrive at Eq. (3.22).

Since the dark sector is decoupled from the visible sector, the initial amount of dark sector particles can be generated by a completely different mechanism than that of the Standard Model particles. For example, if the inflation Hubble parameter H_I is given as $m_s \lesssim H_I \ll M_Q$, the $U(1)_{\rm PQ}$ symmetry is not restored, and s and a are all light particles during inflation. The stochastic fluctuations of the scalar field during inflation $\delta s \sim H_I/2\pi$ can yield its initial abundance after inflation. From Eq. (3.89), these scalars will eventually decay mostly to axions and partially to dark gluons as $\mathrm{Br}(s \to gg) \sim (Ng^2/8\pi^2)^2$ with a total decay rate $\Gamma_s \sim m_s^3/8\pi f_a^2$. Gluons will be quickly thermalized and form thermal bath with a temperature T_g, while the axions are just redshifted. Although this is just one of the production mechanisms for dark sector, it gives a good motivation to study the isocurvature perturbation of dark matter from the initial dark gluon temperature fluctuation $\delta T_{g,i}$. In this case, in addition to the adiabatic perturbation, there are two sources of the isocurvature perturbation. One is the fluctuation of the axion field during the inflation $\delta\phi_i$, and the other is the fluctuation of the gluon temperature $\delta T_{g,i}$, which is induced by initial perturbation of the decaying scalar as Eq. (3.89). Because the dark axions and the dark gluons are coupled with each other by $\partial V/\partial T_g$ in Eq. (3.46), both perturbations could be important for the final isocurvature perturbation of dark matter.

Based on the evolution of the background dark axion and dark gluon/glueball, we solve the equations for the density perturbations focusing on the effect of isocurvature perturbation transfer and obtain the approximated solutions for the super-horizon modes ($k = 0$), in order to understand the parametric dependence more clearly.

3.5.1 Adiabatic Perturbation

For the evolution of the multicomponent fields or fluids, the perturbations can be decomposed into the curvature (adiabatic) perturbation and the isocurvature (entropy) perturbations. The adiabatic perturbation is the modes perturbed along the direction of the background evolution, so that

$$S_{XY} = \mathcal{H}\left(\frac{\delta\rho_X}{\rho_X'} - \frac{\delta\rho_Y}{\rho_Y'}\right) = 0. \tag{3.90}$$

for any different species X and Y [65–67]. S_{XY} is the relative entropy perturbation, whose name can be easily understood from thermodynamics. For an isolated species which satisfies the continuity equation $\rho_X' + 3\mathcal{H}(\rho_X + p_X) = 0$, the perturbation of the entropy density s_X is given as $\delta s_X/s_X = \mathcal{H}\delta\rho_X/\rho_X'$, hence $S_{XY} = 3\,\delta\ln(s_X/s_Y)$. The adiabatic mode can be described by the evolution of the comoving curvature perturbation [68],

$$\mathcal{R} = \Phi - \frac{\mathcal{H}(\Phi' - \mathcal{H}\Psi)}{\mathcal{H}' - \mathcal{H}^2}\ . \tag{3.91}$$

The corresponding initial condition for the adiabatic mode is derived as

$$\Psi_i = -\Phi_i = -\frac{2}{3}\mathcal{R}_i, \quad \delta_{\gamma,i} = \frac{4}{3}\mathcal{R}_i, \tag{3.92a}$$

$$\delta_{a,i} = -\frac{2\eta_a}{3}\mathcal{R}_i, \quad \delta_{g,i} = \frac{4}{3}\mathcal{R}_i\ , \tag{3.92b}$$

where δ_γ is for the photon fluid, the index i indicates the time at which the initial perturbation is defined. Here we use the axion potential and mass in Eq. (3.29).

From Eq. (3.39) and (3.41), we derive the solutions for the super-horizon modes in radiation-dominated era.

$$\Psi = -\Phi = -\frac{2}{3}\mathcal{R}_i, \quad \delta_\gamma = \frac{4}{3}\mathcal{R}_i \ , \tag{3.93a}$$

$$\delta_a = \left[(1+w_a) - (1-w_a)\frac{m_a'(T_g(\tau))}{3\mathcal{H}m_a(T_g(\tau))}\right]\mathcal{R}_i \ , \tag{3.93b}$$

$$\delta_g = \left[(1+w_g) + \frac{(1-w_a)\rho_a}{\rho_g}\frac{m_a'(T_g(\tau))}{3\mathcal{H}m_a(T_g(\tau))}\right]\mathcal{R}_i \ , \tag{3.93c}$$

where $m_a'(T_g(\tau)) \equiv dm_a(T_g(\tau))/d\tau$. As the scale factor becomes larger than a_{ci}, the terms proportional to m_a' is rapidly vanishing. One can show that from the continuity equation for the coupled gluon-axion fluid,

$$\Delta(\rho_a\delta_a + \rho_g\delta_g)|_{a=a_{ci}^{\pm}} = 0, \tag{3.94}$$

the detailed evolution of $m_a(T_g)$ around $a = a_{ci}$ does not lead to the different final result.

Eq. (3.93) states that the adiabatic perturbation shares same form as $\delta_X = (1+w_X)\mathcal{R}_i$ after the confining phase transition of the dark sector, and no history dependence happens, because $S_{XY} = 0$ holds under the time evolution for the super-horizon modes. This is the characteristic feature of the adiabatic perturbation.

3.5.2 Isocurvature Perturbation

The isocurvature perturbation of dark matter is expressed as

$$(\hat{\delta}_{\rm DM})_{\rm iso} = \frac{\Omega_a}{\Omega_{\rm DM}}(\hat{\delta}_a)_{\rm iso} + \frac{\Omega_g}{\Omega_{\rm DM}}(\hat{\delta}_g)_{\rm iso}, \tag{3.95}$$

where 'hat' denotes the Gaussian random variables satisfying $\langle\hat{\delta}_{a,i}\hat{\delta}_{g,i}\rangle = 0$, and

$$\begin{bmatrix} (\hat{\delta}_a)_{\rm iso} \\ (\hat{\delta}_g)_{\rm iso} \end{bmatrix} = \begin{bmatrix} \mathcal{T}_{aa} & \mathcal{T}_{ag} \\ \mathcal{T}_{ga} & \mathcal{T}_{gg} \end{bmatrix} \begin{bmatrix} \hat{\delta}_{a,i} \\ \hat{\delta}_{g,i} \end{bmatrix}, \tag{3.96}$$

with $\mathcal{T}_{aa} \simeq \mathcal{T}_{gg} \simeq 1$. The off-diagonal elements of the transfer matrix, $\mathcal{T}_{ag}$ and $\mathcal{T}_{ga}$ are determined by Eq. (3.46) as follows.

Induced by the Initial Displacement of the Axion Field

The evolution of the isocurvature perturbation induced by an initial density perturbation of the axion $\delta_{a,i} = 2\,\delta\phi_i/\phi_i$ can be described by the input value of $\delta_{a,i}$ with the condition $\mathcal{R}_i = 0$ and the associated solutions from Eq. (3.46c). For $T_g \gg T_{g,c}$, $\partial V/\partial T_g \approx 0$ and

$$\Psi_i = -\Phi_i = 0, \quad \delta_{\gamma,i} = 0, \quad \delta_{g,i} = 0. \tag{3.97}$$

In the axion dominated dark matter scenario ($\Omega_a \gg \Omega_g$), the dominant contribution is trivial: $(\hat{\delta}_{\rm DM})_{\rm iso} \simeq \hat{\delta}_{a,i}$. In the opposite case ($\Omega_a \ll \Omega_g$), the relevant equation for the glueball isocurvature perturbation induced by that of the axion is

$$\begin{aligned} &\delta_g' + 3\mathcal{H}(c_g^2 - w_g)\delta_g \\ &\simeq \frac{(w_a - 1)\rho_a}{\rho_g}\frac{m_a'(T_g(\tau))}{m_a(T_g(\tau)}\left(1 + 3\mathcal{H}c_g^2\frac{T_g}{T_g'}\right)\delta_{a,i}, \end{aligned} \tag{3.98}$$

where $c_g^2 \equiv (dp_g/d\ln T_g)/(\partial\rho_g/\partial\ln T_g)$. Note that the combination of $1 + 3\mathcal{H}c_g^2 T_g/T_g'$ is vanishing in the limit of $\rho_a/\rho_g = 0$ as

$$\frac{T_g'}{T_g} \simeq \left(\frac{\partial\rho_g}{\partial\ln T_g}\right)^{-1}\frac{d\rho_g}{d\tau} \simeq 3\mathcal{H}c_g^2. \tag{3.99}$$

This implies that the transfer matrix element $\mathcal{T}_{ga}$, which represents the effect of the initial axion isocurvature perturbation to that of the glueball dark matter, is of $\mathcal{O}(\Omega_a^2/\Omega_g^2)$. It is the consequence of the conservation of the gluon/glueball entropy during the evolution. Therefore, the dominant contribution to the isocurvature perturbation of dark matter is just that from the axion subcomponent dark matter. In summary,

$$\begin{aligned} (\hat{\delta}_{\rm DM})_{\rm iso} &\simeq \hat{\delta}_{a,i} \qquad \text{for} \quad \Omega_g \ll \Omega_a, \\ (\hat{\delta}_{\rm DM})_{\rm iso} &\simeq \frac{\Omega_a}{\Omega_{\rm DM}}\hat{\delta}_{a,i} \quad \text{for} \quad \Omega_{\rm a} \ll \Omega_g. \end{aligned} \tag{3.100}$$

Induced by the Initial Fluctuation of the GLuon Temperature

For the initial fluctuation of the gluon temperature $\delta_{g,i} \approx 4\,\delta T_{g,i}/T_{g,i}$, the condition $\mathcal{R}_i = 0$ and $\delta\phi_i = 0$ for the perturbative variables give the following initial values

$$\Psi_i = -\Phi_i = 0, \tag{3.101a}$$

$$\delta_{\gamma,i} = -(N^2-1)r^4\delta_{g,i}\ , \tag{3.101b}$$

$$\delta_{a,i} = -\frac{\eta_a}{2}\delta_{g,i}\ . \tag{3.101c}$$

In the glueball-dominated dark matter case, the contribution of the axion is suppressed by its energy density, so $(\hat{\delta}_{\rm DM})_{\rm iso} \simeq \hat{\delta}_{g,i}$. In the opposite case ($\Omega_g \ll \Omega_a$), the effect of the gluon temperature fluctuation to the axion perturbation can be captured by Eq. (3.43). There are three stages of the axion evolution: (I) slow-rolling period ($H \gg m_a(T_g)$), (II) confining phase transition with the saturation of the axion mass $m_a(T_g) = m_a$, (III) axion oscillating period ($H \ll m_a$). For (I), the axion mass term is negligible and

$$\delta\phi'' + 2\mathcal{H}\delta\phi' + a^2\phi\left(\frac{3c_g^2}{4}\frac{dm_a^2(T_g)}{d\ln T_g}\right)\delta_{g,i} \simeq 0. \tag{3.102}$$

The solution becomes

$$\frac{\delta\phi}{\phi} \simeq \quad \frac{\eta_a}{2(2\eta_a+4)(2\eta_a+5)}\left(\frac{m_a^2(T_g)}{H^2}\right)\delta_{g,i}. \tag{3.103}$$

After the confining phase transition, the perturbation of the axion in the periods (II), (III) obeys the equation of motion without δm_a term,

$$\delta\phi'' + 2\mathcal{H}\delta\phi' + a^2 m_a^2\delta\phi = 0. \tag{3.104}$$

The general solution to Eq. (3.104) can be written as the sum of the Bessel functions

$$\delta\phi = \left(\frac{4H}{m_a}\right)^{\frac{1}{4}}\sum_{\lambda=\pm}\delta\phi_\lambda J_{\lambda/4}\left(\frac{1}{2}\frac{m_a^2}{H^2}\right), \tag{3.105}$$

with the constant coefficients $\delta\phi_\pm$. Matching Eq. (3.103) and Eq. (3.105) at $a = a_{ci}$ determines $\delta\phi_\pm$ and gives the solution for (II) and (III). In the period (III), δ_a is given by

$$\delta_a \simeq \frac{\eta_a}{2\eta_a + 4}\left(\frac{m_a}{H_{ci}}\right)^2 \delta_{g,i}, \tag{3.106}$$

where H_{ci} is the Hubble rate at $a = a_{ci}$. Note that the transfer matrix element $\mathcal{T}_{ag}$ is suppressed by the factor of m_a^2/H_{ci}^2 whenever the axion dominates the dark matter, but no further suppression happens. Therefore,

$$\begin{aligned}(\hat{\delta}_{\rm DM})_{\rm iso} &\simeq \hat{\delta}_{g,i} && \text{for } \Omega_a \ll \Omega_g, \\ (\hat{\delta}_{\rm DM})_{\rm iso} &\simeq \left(\frac{\eta_a}{2\eta_a + 4}\left(\frac{m_a}{H_{ci}}\right)^2 + \frac{\Omega_g}{\Omega_{\rm DM}}\right)\hat{\delta}_{g,i} && \text{for } \Omega_g \ll \Omega_a.\end{aligned} \tag{3.107}$$

3.5.3 Bound of the Isocurvature Perturbation

Since $\delta\phi_i$ and $\delta T_{g,i}$ are independent random fluctuations, the power spectrum can be decomposed as

$$P(k,z) = P_{\mathcal{RR}}(k,z) + \sum_{X=a,g} P_{\mathcal{II},X}(k,z), \tag{3.108}$$

where $X = a, g$ stand for the isocurvature perturbations induced by $\delta_{a,i}$ and $\delta_{g,i}$, respectively. For the decomposition of the power spectrum as $P(k,z) = (2\pi^2/k^3)\mathcal{P}(k)T(k,z)$, we can match the primordial spectrum $\mathcal{P}(k)$ with the values we obtained for the superhorizon modes in the previous section. From the observations, the adiabatic mode is nearly scale-independent. For the isocurvature perturbations produced during the inflation, we can also naturally assume they are nearly scale-invariant,

$$\mathcal{P}_{\mathcal{RR}} = A_s\left(\frac{k}{k_*}\right)^{n_s-1}, \ \mathcal{P}_{\mathcal{II},X} = A_X\left(\frac{k}{k_*}\right)^{n_X-1}, \tag{3.109}$$

where k_* is the pivot scale of the wave number, and parameters $\{A_X, n_X\}$ are constants.

Observation of the CMB presents the upper bound on the isocurvature perturbation [13,69–71]. The constraint is expressed by the bound on the isocurvature fraction $\beta_{\rm iso}$, which is defined by

$$\beta_{\rm iso}(k) \equiv \frac{\mathcal{P}_{\mathcal{I}\mathcal{I}}(k)}{\mathcal{P}_{\mathcal{R}\mathcal{R}}(k) + \mathcal{P}_{\mathcal{I}\mathcal{I}}(k)} \ , \tag{3.110}$$

where $\mathcal{P}_{\mathcal{R}\mathcal{R}}$ and $\mathcal{P}_{\mathcal{I}\mathcal{I}}$ are the power spectra defined in Eq. (3.109). For density perturbations, $\mathcal{P}_{\mathcal{R}\mathcal{R}} = k^3\langle\mathcal{R}_i^2\rangle/2\pi^2$ and $\mathcal{P}_{\mathcal{I}\mathcal{I}} = \sum_X k^3\langle(\hat{\delta}_{\rm DM})^2_{{\rm iso},X}\rangle/2\pi^2$. We focus on the large scales to constrain the primordial perturbation from the CMB data. The constraint on $\beta_{\rm iso}$ for the pivot scale is given by [13]

$$\beta_{\rm iso}(k_* = 0.002\,{\rm Mpc}^{-1}) < 0.035. \tag{3.111}$$

We can compare this constraint with the values of $\beta_{\rm iso}$ in our scenario.

If the axion dominates dark matter, $\Omega_g \ll \Omega_a \simeq \Omega_{\rm DM}$ ($R(r, f_a) < 1$ for Eq. (3.76)), the fraction $\beta_{\rm iso}$ can be expressed as

$$\beta_{\rm iso} \simeq \frac{\delta_{a,i}^2}{\mathcal{R}_i^2} + \left(\frac{\eta_a}{2\eta_a + 4}\Big(\frac{m_a}{H_{ci}}\Big)^2 + \frac{\Omega_g}{\Omega_{\rm DM}}\right)^2 \frac{\delta_{g,i}^2}{\mathcal{R}_i^2}, \tag{3.112}$$

where

$$\frac{m_a}{H_{ci}} \simeq 3R(r, f_a), \quad \frac{\Omega_g}{\Omega_{\rm DM}} \simeq (N^2 - 1)R(r, f_a)^{\frac{3}{2}}. \tag{3.113}$$

Because $R(r, f_a) < 1$, the term proportional to $\Omega_g/\Omega_{\rm DM}$ is always the dominant contribution in the second term of the RHS. In the opposite case, if the glueball is the main dark matter component, $\Omega_a \ll \Omega_g \simeq \Omega_{\rm DM}$ ($R(r, f_a) > 1$), we have

$$\beta_{\rm iso} \simeq \frac{\delta_{g,i}^2}{\mathcal{R}_i^2} + \Big(\frac{\Omega_a}{\Omega_{\rm DM}}\Big)^2 \frac{\delta_{a,i}^2}{\mathcal{R}_i^2}, \tag{3.114}$$

where

$$\frac{\Omega_a}{\Omega_{\rm DM}} \simeq \frac{1}{(N^2 - 1)R(r, f_a)^{\frac{3+\eta_a}{2+\eta_a}}}. \tag{3.115}$$

Although the coupling between the axion and the gluon is key to the amount of axion dark matter, the contributions of the same coupling to the isocurvature perturbation is always subdominant. The perturbation is close to the sum of the independent elements, so it allows a large isocurvature perturbation of the subcomponent dark matter. The effect of such a large isocurvature perturbation is not clear yet. Since the glueballs are strongly self-interacting particles, it may provide non-trivial effects if the glueball is the subcomponent dark matter with a large isocurvature perturbation.

In the following section, we study the somewhat different aspect of the subcomponent glueball dark matter in the late time Universe.

3.6 Subcomponent Glueball DM: Formation of Supermassive Black Hole

The subcomponent self-interacting dark matter can play a certain role in formation of supermassive black holes (SMBH). If the self-interaction is strong enough, the gravo-thermal collapse of the subcomponent dark matter can occur at the center of the dark matter halo, leading to the black hole formation at high redshifts $z \gtrsim 7$ [72]. This can provide a possible explanation of the SMBH observations with masses around $10^9 M_\odot$ at $z \sim 7$. From the quasar obervations, we have the list of SMBHs $(z_{\rm obs}, M_{\rm BH})$ as J1342+0928 $(7.54, 7.8 \times 10^8 M_\odot)$, J1120+0641 $(7.09, 2.0 \times 10^9 M_\odot)$, J2348-3054 $(6.89, 2.1 \times 10^9 M_\odot)$ and also J0100+2802 $(6.3, 1.2 \times 10^{10} M_\odot)$ [73–76].

In the standard mechanism on the formation and growth of black holes, SMBHs efficiently increase their mass by the accretion of baryonic material. However, the rate is limited, because the radiation pressure slows down the absorption. The maximal

growth rate is captured by the Salpeter time based on the Eddington limit [77, 78],

$$t_{\rm Sal} = \frac{\epsilon\sigma_T}{4\pi G m_p} = \left(\frac{\epsilon}{0.1}\right) 45\,{\rm Myr}, \tag{3.116}$$

where ϵ is the efficient factor, m_p is the proton mass. If the seed black hole is generated at t_i with a mass $M_{\rm seed}$,

$$M_{\rm BH}(t) \lesssim M_{\rm seed} e^{\frac{t-t_i}{t_{\rm Sal}}}. \tag{3.117}$$

If the seed black hole is formed at $z = 15$, the maximal black hole mass becomes $(2-6)\times 10^4 M_{\rm seed}$ at $z = 7$. If the seed is formed at $z = 30$, its mass becomes $(6-10)\times 10^5 M_{\rm seed}$. Therefore in order to explain the SMBHs with masses of $\mathcal{O}(10^9 M_\odot)$ at $z \sim 7$, a seed mass should be greater than $(10^4 - 10^5) M_\odot$. This is quite challenging in the standard theory of black hole formation.

On the other hand, by solving the gravo-thermal fluid equations [72] and performing N-body simulation [79] with the assumption that the host halo is isolated, it is shown that such a heavy seed black hole could be generated from the gravo-thermal collapse of the subcomponent dark matter. Given the NFW density profile

$$\rho(r) = \frac{\rho_s}{(r/r_s)(1+r/r_s)^2}, \tag{3.118}$$

for the dominant DM component, the seed black hole is formed with the mass

$$M_{\rm seed} \simeq \beta_1 f_g M_h, \tag{3.119}$$

when the age of the Universe becomes

$$t(z_{\rm col}) = t(z_i) + \Delta t_{\rm col}. \tag{3.120}$$

Here, M_h is the mass of the host halo, z corresponds to the redshift. $t(z_i)$ is the time when the virialized dark matter halo is isolated as we assume. $\Delta t_{\rm col}$ is the duration of the gravo-thermal collapse of the subcomponent dark matter for given

initial conditions. β_1 and $\Delta t_{\rm col}$ are both calculated numerically. The fraction factor $\beta_1 \simeq 0.025/(\ln(1+c) - c/(1+c))$ in [72], where c is the concentration of the NFW profile ($M_h = 4\pi\rho_s r_s^3(\ln(1+c) - c/(1+c))$), and $\beta_1 \simeq 0.006$ in [79]. By comparing the dark matter halo density profiles of two papers, we find that both results are well matched. The formation period $\Delta t_{\rm col}$ is estimated as the form

$$\Delta t_{\rm col} \simeq \beta_2 f_g^{-p} t_{\rm rel} \tag{3.121}$$

where $\beta_2 \simeq 456\,(480)$, $p = 0\,(2)$ in [72] ([79]), and the apparent relaxation time of the subcomponent dark matter at $t = t(z_i)$ is defined as

$$\begin{aligned} t_{\rm rel} &\equiv \frac{m_g}{f_g \sigma_g \rho_s v_s} \\ &= 0.28\,{\rm Myr}\left(\frac{10\,{\rm cm}^2/{\rm g}}{f_g\sigma_g/m_g}\right)\left(\frac{10^9 M_\odot/{\rm kpc}^3}{\rho_s}\right)^{3/2}\left(\frac{3\,{\rm kpc}}{r_s}\right). \end{aligned} \tag{3.122}$$

σ_g is the elastic scattering cross-section between two subcomponent dark matters (dark glueballs in our case), v_s is the virialized velocity at $r = r_s$. Then the seed black hole can form after the period

$$\begin{aligned} \Delta t_{\rm col} \;\simeq\; & 130\,{\rm Myr}\left(\frac{10\,{\rm cm}^2/{\rm g}}{f_g^{p+1}\sigma_g/m_g}\right) \\ & \times\left(\frac{10^9 M_\odot/{\rm kpc}^3}{\rho_s}\right)^{3/2}\left(\frac{3\,{\rm kpc}}{r_s}\right). \end{aligned} \tag{3.123}$$

Note that $\Delta t_{\rm col}$ can be shorter than the age of the Universe for a given z, $t(z) \simeq 550\,{\rm Myr}(\frac{10}{1+z})^{3/2}$. Therefore, for the isolated halo with a mass $M_h = 10^{12} M_\odot$, $f_g^{p+1}\sigma_g/m_g \gtrsim (1-10)\,{\rm cm}^2/{\rm g}$, and $f_g \lesssim 0.001 - 0.01$ can explain the SMBH around $z = 7$. We illustrate the formation of the seed black hole and its growth history in Fig. 3.7 for the halo mass $M_h = 10^{12} M_\odot$. Fig. 3.8 also shows the change in the central density profile of sub-component self-interacting dark matter halo by the gravo-thermal collapse from N-body simulation.

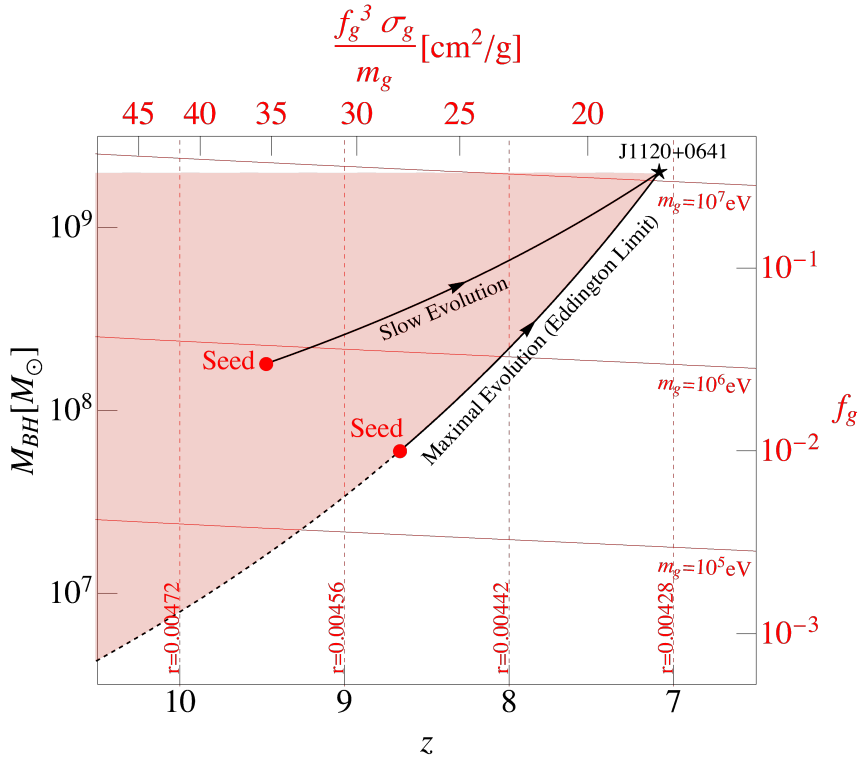

Figure 3.7 Illustration of the black hole growth history for the observed high z black hole $J1120+0641$ with the assumption of the isolated host halo ($M_h = 10^{12} M_\odot$) as [72, 79]. All information in red illustrates parameter space for a seed black hole (red dot). The seed black hole can be on the Eddington curve or on the shaded area in which the observations are explained by slower growth of the seed black hole. The time of collapse ($z_{\rm col}$) and the mass of the seed black hole $M_{\rm seed}$ are determined by model parameters $\{f_g, \sigma_g/m_g\}$ or $\{m_g, r\}$.

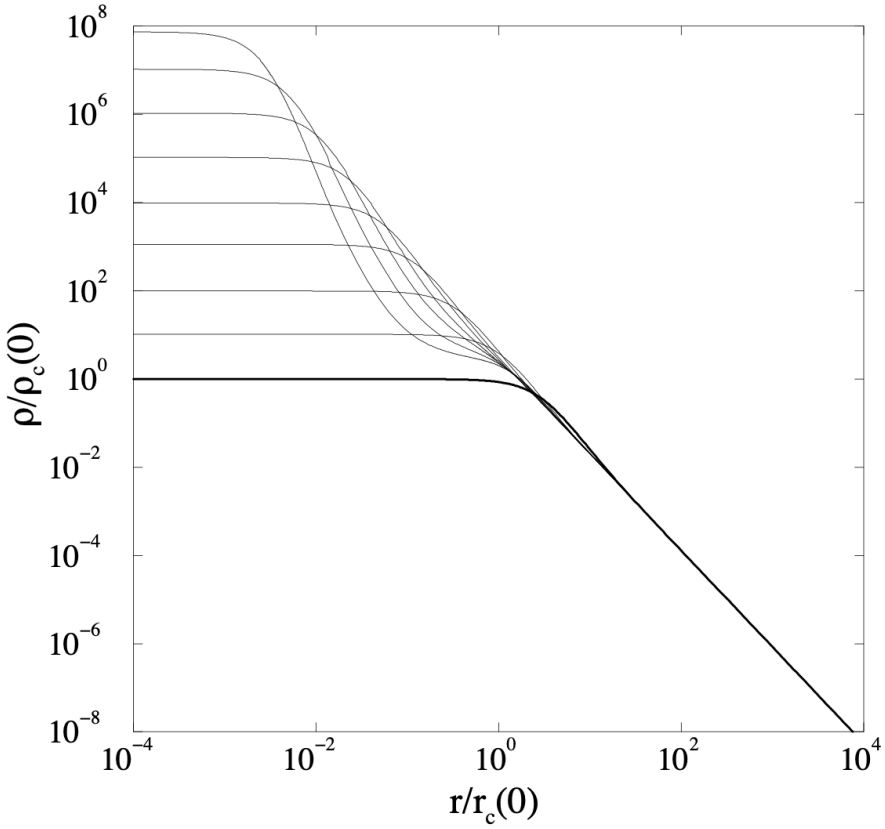

Figure 3.8 Change in the central density profile of sub-component self-interacting dark matter halo by the gravothermal collapse from N-body simulation, from Ref. [80]. The SIDM halo becomes more concentrated via gravo-thermal process.

In our scenario, the dark glueball dark matter provides a such strongly interacting subcomponent dark matter. Since β_2 and p are directly estimated in N-body simulation, we take the result of [79] ($\beta_2 = 480$, $p = 2$) as the benchmark value. Then, the relevant combination of the model parameters is $f_g^3\sigma_g/m_g$, which is estimated as

$$\begin{aligned}\frac{f_g^3\sigma_g}{m_g} &= \left(\frac{3}{N}\right)^4\left(\frac{f_g}{m_g}\right)^3 \\ &\simeq 40\,\mathrm{cm}^2/\mathrm{g}\left(\frac{3}{N}\right)^4\left(\frac{N^2-1}{10}\right)^3\left(\frac{r}{0.005}\right)^9. \end{aligned} \tag{3.124}$$

For the final expression, Eq. (3.85) is used. Because it is very sensitive to r, the ratio parameter is nearly predicted from the explanation of the SMBH at high z. The corresponding allowed range of the glueball mass is also provided as $m_g = \mathcal{O}(0.05)$MeV for $f_g = \mathcal{O}(0.001)$. As to the parameters of the dominant component of dark matter, the axion, its decay constant is $f_a = \mathcal{O}(10^{16}\,\mathrm{GeV})$ and the axion mass becomes $m_a = \mathcal{O}(10^{-18})\,\mathrm{eV}$. This is safe from the current fuzzy dark matter constraints. Interestingly, this axion mass is also related with the supermassive black hole with the mass of $M_{\mathrm{BH}} \sim 10^7 M_\odot$ through superradiance as we discussed before. The axions can be efficiently generated from the spinning black hole by superradiant amplification. During the amplification, the axion also takes away the sizable amount of the black hole's angular momentum, which gives the contradiction to the observation [81]. However, if the self-interaction among the axions is sizable, they will collapse before the axion cloud is saturated [82], and the loss of the angular momentum is limited. For $m_a \sim 10^{-18}\,\mathrm{eV}$, the GUT scale decay constant provides a sizable axion self-interaction to trigger bosenovae. Therefore, the constraint may not be applied directly.

Several simplications are used in the previous discussion. Let us discuss possible caveats and alternative history of the seed black hole formation. The host halo mass is taken as $10^{12}M_\odot$. This is because the halo mass is expected to be greater than $\mathcal{O}(10^3)$ times the mass of its SMBH [83, 84]. In N-body simulations [85–87], the comoving

number density of the cold dark matter halos with $M_h \geq 10^{12} M_\odot$ is evaluated as $(10^{-5} - 10^{-6})(\mathrm{Mpc})^{-3}$ at $z = 7$. Thus, the halo is also heavy enough to coincide with the fact that observations of SMBH around $z = 7$ are rare.

However, since we consider the formation of the seed black hole at higher redshifts ($z > 7$), the existence of such (isolated) heavy halo is questionable. If we extrapolate the halo mass function obtained by the N-body simulation (Fig. 3.9) [87], the comoving number density of the halos with $M_h \geq 10^{12} M_\odot$ becomes $(10^{-8} - 10^{-9})(\mathrm{Mpc})^{-3}$ at $z = 10$, and $10^{-15}(\mathrm{Mpc})^{-3}$ at $z = 15$. In this context, the issue of formation of heavy seed black holes is just transferred to the problem of supermassive halo formation at high redshifts.

On one hand, based on N-body simulations, we can define $M_h(z)$ at a given z in such a way that the comoving number density of the halos with their masses greater than $M_h(z)$ is given by $10^{-6}(\mathrm{Mpc})^{-3}$. Then, $M_h(z)$ is evaluated as $10^{12} M_\odot$ at $z = 7$, $10^{11} M_\odot$ at $z = 10$, and $10^{10} M_\odot$ at $z = 15$. It is more natural to think the possibility that when the seed black hole is formed, the mass of the host halo is smaller than $10^{12} M_\odot$, although it is still one of the heaviest halos at z_i. These heaviest halos get bigger and bigger by mergers with nearby smaller halos or by accretion of the gases. The actual merger history is quite complex, but the heaviest halo is likely to remain the heaviest. In this sense, we consider $M_h(z)$ as the evolution of the host halo mass, and estimate the growth rate $\Gamma_h(z)$ as

$$\Gamma_h(z) \equiv \frac{1}{M_h(z)} \frac{dM_h(z)}{dt} \simeq \frac{4}{t(z)}. \tag{3.125}$$

The last equality holds numerically for $7 \lesssim z \lesssim 15$. The black hole growth rate by the accretion of baryons is much greater than the halo growth rate. However, the halo mass is still hierarchically larger than the black hole mass during the evolution.

The another important feature is that in terms of the halo mass, the relaxation

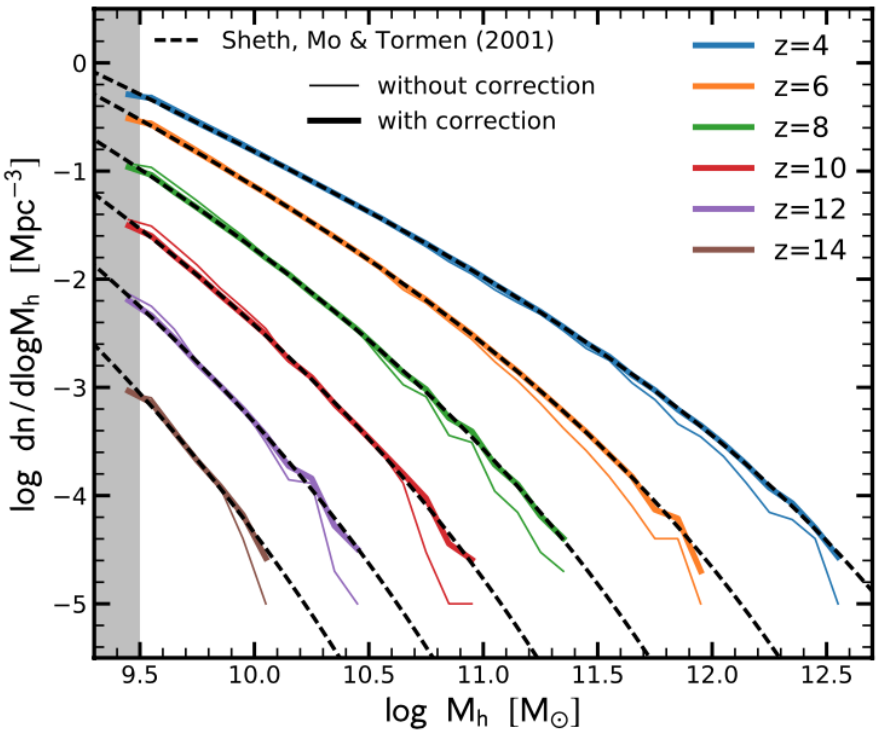

Figure 3.9 Halo mass function for different redshifts from N-body simulation, from Ref. [87].

time defined by Eq. (3.122) depends on z, c and M_h as

$$t_{\rm rel} \propto \frac{(\ln(1+c) - \frac{c}{1+c})^{\frac{3}{2}}}{(1+z)^{\frac{7}{2}} c^{\frac{7}{2}} M_h^{\frac{1}{3}}}. \tag{3.126}$$

The concentration parameter c also depends on the halo mass and the redshift. The recent N-body simulation [88] calculates the concentration parameter $c(M_h, z)$ as the function of M_h and z in a wide range of M_h and z. With the reasonable extrapolation, we find $c(10^{10} M_\odot, 13.8) \simeq c(10^{11} M_\odot, 9.5) \simeq c(10^{12} M_\odot, 7) = 4 - 5$. Thus, $c(M_h(z), z)$ does not have significant z dependence. Including all these considerations, Fig. 3.10 shows the apparent gravo-thermal collapse period $\Delta t_{\rm col}$ as the function of M_h and z

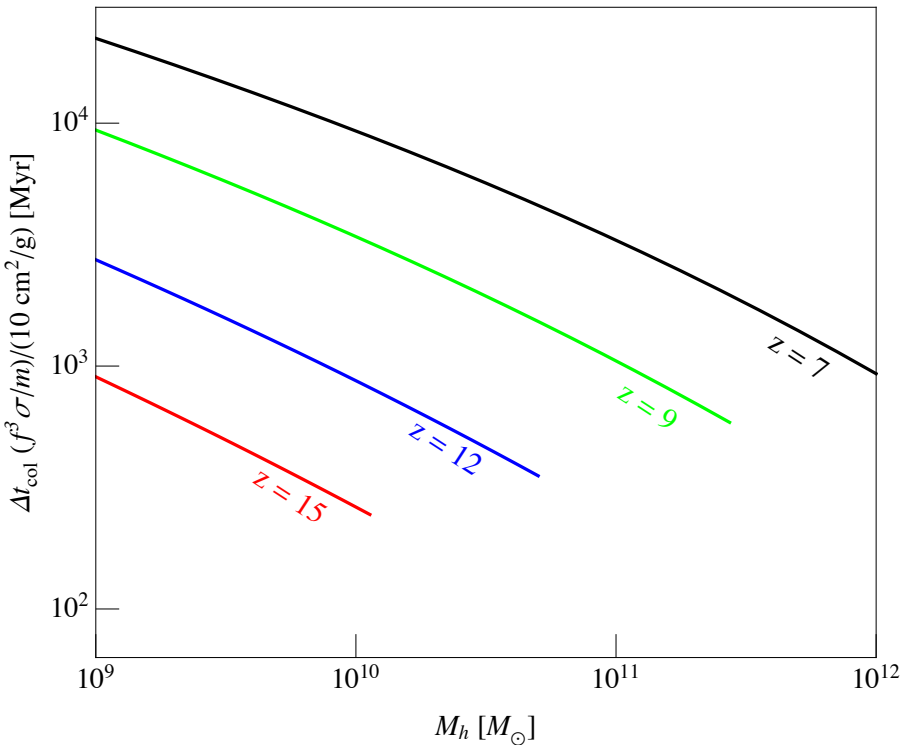

Figure 3.10 The expected duration of the gravo-thermal collapse of the subcomponent dark matter $\Delta t_{\rm col}$ in the unit of $(f_g^3\sigma_g/m_g)^{-1}$, defined as Eqs. (3.121) and (3.122) with $\beta_2 = 480$, $p = 2$. It is plotted for the different halo masses and redshifts based on the NFW profile of the dominant dark matter component with the fitted concentration parameter $c(M_h, z)$ [88]. The end point of each line corresponds to the halo mass $M_h = M_h(z)$. The actual collapse time of the subcomponent dark matter will depend on the halo growth history.

in the unit of $(f_g^3\sigma_g/m_g)^{-1}$. The formation of the seed black hole is more efficient for heavier halos at a given z. In order to see whether or not the early formation of the seed is preferred (z-dependence), we have to compare $\Delta t_{\rm col}$ with the Hubble time. Numerically, we find that the z dependence of $\Delta t_{\rm col}$ for $M_h = M_h(z)$ approximately scales as $1/(1+z)^{1.5}$ in the range $z = 7 - 15$ like the Hubble time. Therefore, if the seed black hole can form, the formation happens at earlier time with a smaller mass.

Even if $\Delta t_{\rm col}$ is shorter than the age of the Universe at z_i, the isolated halo assumption may not be valid if the period of the gravo-thermal collapse is longer than the halo growth time scale $1/\Gamma_h$. The general expectation is that the merger process will hinder the gravo-thermal collapse. We consider the conservative criterion for the formation of the seed black hole as

$$\Gamma_h(z)\Delta t_{\rm col}(z) \lesssim 4\Delta t_{\rm col}(z)/t(z) \lesssim 1. \tag{3.127}$$

This condition means that the seed black hole can only form when the collapse process is faster than the growth rate of the halo mass. We take $z_i = 15$ as the initial redshift for the virialized heaviest host halo. Then, Eq. (3.127) is satisfied if

$$\frac{f_g^3\sigma_g}{m_g} \gtrsim 40\,{\rm cm}^2/{\rm g}. \tag{3.128}$$

After the seed black hole is formed around $z = 15$, its mass is exponentially growing, and it becomes $M_{\rm BH} = 10^9 M_\odot$ at $z = 7$ if the fraction of the glueball dark matter is given as $f_g = 2 \times 10^{-4}$. This is the case of the fastest growth, so the lower bound of f_g to explain current observations of the SMBHs is given by

$$f_g \gtrsim 2 \times 10^{-4}\ . \tag{3.129}$$

So far, we have ignored the effect of the number-changing interactions of the dark glueballs during the gravo-thermal collapse. If the number-changing process becomes efficient as the density increases, the sizable pressure of the glueballs may disturb the

collapse. To simplify our discussion, in terms of the temperature of the glueball dark matter (T_g) inside the dark matter halo ($r < r_s$), there are two totally different sources to increase T_g. One is the gravo-thermal collapse. Because the gravitationally bound system has a negative specific heat, as heat flows outward, the glueballs become more and more concentrated in a smaller volume with a larger virial velocity. This results in temperature increasing, and leads to the collapse as the heat outflow accelerates. On the other hand, the $3 \to 2$ scatterings directly produce the large kinetic energies of the daughter glueballs as $E_{\rm kin} \simeq m_g/2$, respectively. These energies will be redistributed among glueballs within the relaxation time, so that the overall glueball temperature will increase compared to the virial temperature, and inhibit to collapse.

In order to figure out the condition that the gravo-thermal collapse can start, we require a criterion that the rate of glueball temperature increase is small enough to satisfy

$$\frac{\Delta t_{\rm col}}{T_g}\Big(\frac{dT_g}{dt}\Big)_{3\to 2} \ll 1. \tag{3.130}$$

The temperature increase rate by the three-to-two scatterings is estimated for the given glueball density ρ_g and the velocity v_g

$$\frac{1}{T_g}\Big(\frac{dT_g}{dt}\Big)_{3\to 2} = \xi_{\rm eff}\langle\sigma_{3\to 2}v_g^2\rangle n_g^2\frac{m_g}{T_g} \simeq \frac{\langle\sigma_{3\to 2}v_g^2\rangle\rho_g^2}{m_g^2\langle v_g^2\rangle}, \tag{3.131}$$

where $T_g = m_g\langle v_g^2\rangle$, $\xi_{\rm eff}$ is the efficiency factor of the energy redistribution. $\xi_{\rm eff}$ could be suppressed if the mean-free path of the glueball is much larger than the size of the core. In our case, most of the glueballs are trapped by the elastic scattering, so $\xi_{\rm eff} \simeq 1$. Before the gravo-thermal collapse accelerates, the glueball density and the velocity are not much changed. For $\rho_g = f_g\rho_s$, $v_g = v_s$,

$$\begin{aligned}\frac{\Delta t_{\rm col}}{T_g}\left(\frac{dT_g}{dt}\right)_{3\to 2} &\simeq 0.06\Big(\frac{10^{-3}}{f_g}\Big)\Big(\frac{3}{N}\Big)^2\Big(\frac{10^{-3}}{v_s}\Big)^2 \\ &\quad\times\Big(\frac{\rm keV}{m_g}\Big)^4\Big(\frac{\rho_s}{10^{12}M_\odot/{\rm kpc}^3}\Big).\end{aligned} \tag{3.132}$$

Therefore, we expect that the gravo-thermal collapse for the SMBH would not be triggered if $m_g \lesssim$ keV.

If m_g is much larger than $\mathcal{O}$(keV), the three-to-two interaction is not effective before the gravo-thermal collapse happens. The gravo-thermal collapse begins to accelerate after $\Delta t_{\rm col}$. During the collapse, the diffusion of the dark matter mass is inefficient, and the glueballs concentrate their mass of $\mathcal{O}(M_{\rm seed})$ around the center by increasing the core density and its temperature [80, 89]. Then, the number changing interaction becomes gradually important. It is not clear how it affects the last stage of the gravo-thermal collapse (the formation of the seed black hole). This is because the temperature increase rate caused by gravo-thermal collapse is not known yet for such a high mass density of the core. We leave it for future work.

There is also the lower bound on the glueball mass from the cosmological evolution. If the glueball is light enough, it becomes a warm or hot dark matter, so that its speed around $z = 7 - 15$ is greater than the escape velocity of the halo. This means that the subcomponent dark matter is not clustered, and cannot provide a good initial condition. After the dark glueball freeze-out, its velocity scales as $1/a$. The corresponding redshifted glueball velocity at a given z is

$$v_g(z) \simeq 10^{-3} \left(\frac{1+z}{16}\right) \left(\frac{r}{0.001}\right)^{\frac{3}{2}} \left(\frac{100\,\mathrm{eV}}{m_g}\right)^{\frac{5}{4}}, \tag{3.133}$$

if the freeze-out happens before the epoch of matter-radiation equality, and

$$v_g(z) \simeq 10^{-3} \left(\frac{1+z}{16}\right) \left(\frac{r}{0.001}\right)^{\frac{4}{3}} \left(\frac{100\,\mathrm{eV}}{m_g}\right)^{\frac{10}{9}}, \tag{3.134}$$

if the freeze-out happens in the dark matter dominated era. In order to explain the SMBH formation, this value should be hierarchically smaller than the virial velocity $v_s \sim 10^{-3}$ during the period $z = 7 - 15$. In our scenario, r is nearly fixed as 0.005. See Eq. (3.124). This implies the lower bound on m_g as 100 eV.

Chapter 4

Conclusion and Discussion

We have studied the cosmological evolution and implications of light scalar dark matters. For the light scalars, we consider two cases with naturally small mass. The first case is a pseudo-Goldstone boson, whose mass originate from the approximate global symmetry. The second case is a composite particle in an asymptotically free gauge sector, so its mass is given by the confining scale of the gauge sector. Both can be incorporated in a simple set-up of the dark Yang-Mills gauge sector. The former is the feebly interacting dark axion coupled to the gauge sector and the other is the strongly interacting dark glueballs.

The equations of motion are derived and evaluated to identify the dark matter abundance. The dark axion behaves like a dark energy before it starts oscillating. After it starts coherent oscillation, it becomes a cold dark matter. There is open parameter space for the dark axion to be a fuzzy dark matter. The dark glueballs act as cannibalistic dark matters with strong number-changing self-interaction. Their energy density evolves non-trivially as the universe expands.

The dark axion coupled to the confining gauge sector gets its potential through the interaction with the dark gluon. It leads to the axion potential that depends on temperature of the gluon. The impact of the temperature dependent axion potential is taken into account in the equations of the perturbation evolution. As a result, the initial isocurvature perturbation induced by the initial fluctuation of the gluon temperature can yield the density perturbation of the axion. We also explore the possibility that the subcomponent glueball dark matter contributes to the formation of the observed supermassive black holes at redshift $z \sim 7$.

Although we have dealt with the problems as closely as possible, there are still many questions that have not been covered by this paper. What would be the observable consequences of the first-order confining phase transition? In our discussion, we ignore gravitational wave productions during the confining phase transition, because it is weakly first-order unless N is very large. However, if the phase transition happens around the recombination era, it may leave a footprint on the CMB. What is the exact form of the axion scalar potential and the effect of self-interactions? The scalar potential of the axion is not a simple cosine form, and a multi-branch structure may provide the nontrivial effects if the axion is produced around the spinning supermassive black hole by superradiant amplification. What is the correct period of the gravo-thermal collapse when the fraction of the subcomponent dark matter is small enough? So far, there is no intensive study on the gravo-thermal collapse of the subcomponent dark matter for such a small fraction. The empirical form of the collapse time scale $\Delta t_{\rm col}$ should be confirmed for $f_g \ll 10\%$ and higher scattering cross-sections. What is the effect of the number changing interactions of the glueball dark matter for the final stage of the black hole formation? During the gravo-thermal collapse, one may think of the possibility that the defining phase transition occurs, because of the large density of the glueball dark matter inside the core. It would be very interesting to study the implication of such a microscopic nature of the dark

matter for the final formation of the black hole.

Bibliography

[1] V. M. Slipher, *The radial velocity of the Andromeda Nebula*, *Lowell Observatory Bulletin* **1** (1913) 56.

[2] V. M. Slipher, *Spectrographic Observations of Nebulae*, *Popular Astronomy* **23** (1915) 21.

[3] E. Hubble, *A Relation between Distance and Radial Velocity among Extra-Galactic Nebulae*, *Proceedings of the National Academy of Science* **15** (1929) 168.

[4] E. E. Falco, M. J. Kurtz, M. J. Geller, J. P. Huchra, J. Peters, P. Berlind et al., *The Updated Zwicky Catalog (UZC)*, *Publ. Astron. Soc. Pac.* **111** (1999) 438 [astro-ph/9904265].

[5] M. Colless, *First results from the 2dF galaxy redshift survey*, *Phil. Trans. Roy. Soc. Lond. A* **357** (1999) 105 [astro-ph/9804079].

[6] SDSS-IV collaboration, R. Ahumada et al., *The 16th Data Release of the Sloan Digital Sky Surveys: First Release from the APOGEE-2 Southern Survey and Full Release of eBOSS Spectra*, *Astrophys. J. Suppl.* **249** (2020) 3 [1912.02905].

[7] Particle Data Group collaboration, M. Tanabashi et al., *Review of Particle Physics*, *Phys. Rev. D* **98** (2018) 030001.

[8] Planck collaboration, N. Aghanim et al., *Planck 2018 results. VI. Cosmological parameters*, *Astron. Astrophys.* **641** (2020) A6 [1807.06209].

[9] Planck collaboration, P. Ade et al., *Planck 2015 results. XIII. Cosmological parameters*, *Astron. Astrophys.* **594** (2016) A13 [1502.01589].

[10] M. Pospelov and J. Pradler, *Big Bang Nucleosynthesis as a Probe of New Physics*, *Ann. Rev. Nucl. Part. Sci.* **60** (2010) 539 [1011.1054].

[11] Particle Data Group collaboration, P. Zyla et al., *Review of Particle Physics*, *PTEP* **2020** (2020) 083C01.

[12] E. W. Kolb and M. S. Turner, *The Early Universe*, vol. 69. 1990.

[13] Planck collaboration, Y. Akrami et al., *Planck 2018 results. X. Constraints on inflation*, 1807.06211.

[14] S. Dodelson, *Modern Cosmology*. Academic Press, Amsterdam, 2020.

[15] D. Baumann and H. V. Peiris, *Cosmological Inflation: Theory and Observations*, *Adv. Sci. Lett.* **2** (2009) 105 [0810.3022].

[16] L. Verde, T. Treu and A. Riess, *Tensions between the Early and the Late Universe*, 7, 2019, 1907.10625, DOI.

[17] J. Dubinski and R. G. Carlberg, *The Structure of Cold Dark Matter Halos*, *Astrophys. J.* **378** (1991) 496.

[18] J. F. Navarro, C. S. Frenk and S. D. M. White, *The Structure of Cold Dark Matter Halos*, *Astrophys. J.* **462** (1996) 563 [astro-ph/9508025].

[19] B. Moore, T. Quinn, F. Governato, J. Stadel and G. Lake, *Cold collapse and the core catastrophe*, *Mon. Not. R. Astron. Soc.* **310** (1999) 1147 [astro-ph/9903164].

[20] S.-H. Oh, W. J. G. de Blok, E. Brinks, F. Walter and R. C. Kennicutt, *Dark and luminous matter in things dwarf galaxies*, *The Astronomical Journal* **141** (2011) 193.

[21] B. Moore, S. Ghigna, F. Governato, G. Lake, T. Quinn, J. Stadel et al., *Dark matter substructure within galactic halos*, *The Astrophysical Journal* **524** (1999) L19–L22.

[22] A. Klypin, A. V. Kravtsov, O. Valenzuela and F. Prada, *Where are the missing galactic satellites?*, *The Astrophysical Journal* **522** (1999) 82–92.

[23] G. 't Hooft, *A Planar Diagram Theory for Strong Interactions*, *Nucl. Phys. B* **72** (1974) 461.

[24] E. Witten, *Baryons in the 1/n Expansion*, *Nucl. Phys. B* **160** (1979) 57.

[25] A. Manohar and H. Georgi, *Chiral Quarks and the Nonrelativistic Quark Model*, *Nucl. Phys. B* **234** (1984) 189.

[26] A. G. Cohen, D. B. Kaplan and A. E. Nelson, *Counting 4 pis in strongly coupled supersymmetry*, *Phys. Lett. B* **412** (1997) 301 [hep-ph/9706275].

[27] E. Witten, *Large N Chiral Dynamics*, *Annals Phys.* **128** (1980) 363.

[28] E. Witten, *Theta dependence in the large N limit of four-dimensional gauge theories*, *Phys. Rev. Lett.* **81** (1998) 2862 [hep-th/9807109].

[29] L. Del Debbio, G. M. Manca, H. Panagopoulos, A. Skouroupathis and E. Vicari, *Theta-dependence of the spectrum of SU(N) gauge theories*, *JHEP* **06** (2006) 005 [hep-th/0603041].

[30] E. Vicari and H. Panagopoulos, *Theta dependence of SU(N) gauge theories in the presence of a topological term*, *Phys. Rept.* **470** (2009) 93 [0803.1593].

[31] D. J. Gross, R. D. Pisarski and L. G. Yaffe, *Qcd and instantons at finite temperature*, *Rev. Mod. Phys.* **53** (1981) 43.

[32] S. Borsanyi et al., *Calculation of the axion mass based on high-temperature lattice quantum chromodynamics*, *Nature* **539** (2016) 69 [1606.07494].

[33] N. Bartolo, P. S. Corasaniti, A. R. Liddle and M. Malquarti, *Perturbations in cosmologies with a scalar field and a perfect fluid*, *Phys. Rev. D* **70** (2004) 043532 [astro-ph/0311503].

[34] W. Hu, *Structure formation with generalized dark matter*, *Astrophys. J.* **506** (1998) 485 [astro-ph/9801234].

[35] C.-P. Ma and E. Bertschinger, *Cosmological perturbation theory in the synchronous and conformal Newtonian gauges*, *Astrophys. J.* **455** (1995) 7 [astro-ph/9506072].

[36] L. D. McLerran, E. Mottola and M. E. Shaposhnikov, *Sphalerons and Axion Dynamics in High Temperature {QCD}*, *Phys. Rev. D* **43** (1991) 2027.

[37] G. D. Moore and M. Tassler, *The Sphaleron Rate in SU(N) Gauge Theory*, *JHEP* **02** (2011) 105 [1011.1167].

[38] Y. Deng, *The energy density and pressure in su(3) lattice gauge theory at finite temperature*, *Nuclear Physics B - Proceedings Supplements* **9** (1989) 334 .

[39] S. Datta and S. Gupta, *Continuum Thermodynamics of the GluoN_c Plasma*, *Phys. Rev. D* **82** (2010) 114505 [1006.0938].

[40] S. Borsanyi, G. Endrodi, Z. Fodor, S. Katz and K. Szabo, *Precision SU(3) lattice thermodynamics for a large temperature range*, *JHEP* **07** (2012) 056 [1204.6184].

[41] M. J. Teper, *Physics from the lattice: Glueballs in QCD: Topology: SU(N) for all N*, in *NATO Advanced Study Institute on Confinement, Duality and Nonperturbative Aspects of QCD*, pp. 43–74, 6, 1997, hep-lat/9711011.

[42] M. J. Teper, *Glueball masses and other physical properties of SU(N) gauge theories in D = (3+1): A Review of lattice results for theorists*, hep-th/9812187.

[43] C. J. Morningstar and M. J. Peardon, *The Glueball spectrum from an anisotropic lattice study*, *Phys. Rev. D* **60** (1999) 034509 [hep-lat/9901004].

[44] A. Athenodorou and M. Teper, *The glueball spectrum of SU(3) gauge theory in 3+1 dimension*, 2007.06422.

[45] B. Lucini and G. Moraitis, *The Running of the coupling in SU(N) pure gauge theories*, *Phys. Lett. B* **668** (2008) 226 [0805.2913].

[46] B. Lucini, A. Rago and E. Rinaldi, *SU(N_c) gauge theories at deconfinement*, *Phys. Lett. B* **712** (2012) 279 [1202.6684].

[47] B. Lucini, A. Rago and E. Rinaldi, *Glueball masses in the large N limit*, *JHEP* **08** (2010) 119 [1007.3879].

[48] M. Caselle, A. Nada and M. Panero, *Hagedorn spectrum and thermodynamics of SU(2) and SU(3) Yang-Mills theories*, *JHEP* **07** (2015) 143 [1505.01106].

[49] L. Forestell, D. E. Morrissey and K. Sigurdson, *Non-Abelian Dark Forces and the Relic Densities of Dark Glueballs*, *Phys. Rev. D* **95** (2017) 015032 [1605.08048].

[50] C. Bonati, M. D'Elia, P. Rossi and E. Vicari, *Theta dependence in the large N limit*, *PoS* **LATTICE2016** (2017) 348 [1702.01049].

[51] D. Gaiotto, A. Kapustin, Z. Komargodski and N. Seiberg, *Theta, Time Reversal, and Temperature*, *JHEP* **05** (2017) 091 [1703.00501].

[52] S. Dubovsky, A. Lawrence and M. M. Roberts, *Axion monodromy in a model of holographic gluodynamics*, *JHEP* **02** (2012) 053 [1105.3740].

[53] F. Bigazzi, A. L. Cotrone and R. Sisca, *Notes on Theta Dependence in Holographic Yang-Mills*, *JHEP* **08** (2015) 090 [1506.03826].

[54] S. Tulin and H.-B. Yu, *Dark Matter Self-interactions and Small Scale Structure*, *Phys. Rept.* **730** (2018) 1 [1705.02358].

[55] B. S. Acharya, M. Fairbairn and E. Hardy, *Glueball dark matter in non-standard cosmologies*, *JHEP* **07** (2017) 100 [1704.01804].

[56] D. Grin, M. A. Amin, V. Gluscevic, R. Hlǒzek, D. J. Marsh, V. Poulin et al., *Gravitational probes of ultra-light axions*, 1904.09003.

[57] E. G. Ferreira, *Ultra-Light Dark Matter*, 2005.03254.

[58] R. Brito, V. Cardoso and P. Pani, *Superradiance: Energy Extraction, Black-Hole Bombs and Implications for Astrophysics and Particle Physics*, vol. 906. Springer, 2015, 10.1007/978-3-319-19000-6, [1501.06570].

[59] R. Hlozek, D. J. E. Marsh and D. Grin, *Using the Full Power of the Cosmic Microwave Background to Probe Axion Dark Matter*, *Mon. Not. Roy. Astron. Soc.* **476** (2018) 3063 [1708.05681].

[60] W. Hu, R. Barkana and A. Gruzinov, *Cold and fuzzy dark matter*, *Phys. Rev. Lett.* **85** (2000) 1158 [astro-ph/0003365].

[61] J.-c. Hwang and H. Noh, *Axion as a Cold Dark Matter candidate*, *Phys. Lett. B* **680** (2009) 1 [0902.4738].

[62] V. Iršič, M. Viel, M. G. Haehnelt, J. S. Bolton and G. D. Becker, *First constraints on fuzzy dark matter from Lyman-α forest data and hydrodynamical simulations*, *Phys. Rev. Lett.* **119** (2017) 031302 [1703.04683].

[63] A. Soni and Y. Zhang, *Hidden SU(N) Glueball Dark Matter*, *Phys. Rev. D* **93** (2016) 115025 [1602.00714].

[64] M. A. Buen-Abad, R. Emami and M. Schmaltz, *Cannibal Dark Matter and Large Scale Structure*, *Phys. Rev. D* **98** (2018) 083517 [1803.08062].

[65] A. R. Liddle, D. H. Lyth, K. A. Malik and D. Wands, *Superhorizon perturbations and preheating*, *Phys. Rev. D* **61** (2000) 103509 [hep-ph/9912473].

[66] D. Wands, K. A. Malik, D. H. Lyth and A. R. Liddle, *A New approach to the evolution of cosmological perturbations on large scales*, *Phys. Rev. D* **62** (2000) 043527 [astro-ph/0003278].

[67] S. Weinberg, *Adiabatic modes in cosmology*, *Phys. Rev. D* **67** (2003) 123504 [astro-ph/0302326].

[68] V. F. Mukhanov, H. Feldman and R. H. Brandenberger, *Theory of cosmological perturbations. Part 1. Classical perturbations. Part 2. Quantum theory of perturbations. Part 3. Extensions*, *Phys. Rept.* **215** (1992) 203.

[69] P. Crotty, J. Garcia-Bellido, J. Lesgourgues and A. Riazuelo, *Bounds on isocurvature perturbations from CMB and LSS data*, *Phys. Rev. Lett.* **91** (2003) 171301 [astro-ph/0306286].

[70] H. Li, J. Liu, J.-Q. Xia and Y.-F. Cai, *Cold Dark Matter Isocurvature Perturbations: Cosmological Constraints and Applications*, *Phys. Rev. D* **83** (2011) 123517 [1012.2511].

[71] J. Väliviita and V. Muhonen, *Correlated adiabatic and isocurvature cosmic microwave background fluctuations in the wake of the results from the wilkinson microwave anisotropy probe*, *Phys. Rev. Lett.* **91** (2003) 131302.

[72] J. Pollack, D. N. Spergel and P. J. Steinhardt, *Supermassive Black Holes from Ultra-Strongly Self-Interacting Dark Matter*, *Astrophys. J.* **804** (2015) 131 [1501.00017].

[73] D. J. Mortlock, S. J. Warren, B. P. Venemans, M. Patel, P. C. Hewett, R. G. McMahon et al., *A luminous quasar at a redshift of z = 7.085*, *Nature* **474** (2011) 616–619.

[74] G. De Rosa et al., *Black hole mass estimates and emission-line properties of a sample of redshift z¿6.5 quasars*, *Astrophys. J.* **790** (2014) 145 [1311.3260].

[75] X.-B. Wu, F. Wang, X. Fan, W. Yi, W. Zuo, F. Bian et al., *An ultra-luminous quasar with a twelve-billion-solar-mass black hole at redshift 6.30*, *Nature* **518** (2015) 512.

[76] E. Banados et al., *An 800-million-solar-mass black hole in a significantly neutral Universe at redshift 7.5*, *Nature* **553** (2018) 473 [1712.01860].

[77] E. Salpeter, *Accretion of Interstellar Matter by Massive Objects*, *Astrophys. J.* **140** (1964) 796.

[78] M. Volonteri, *Formation of supermassive black holes*, *The Astronomy and Astrophysics Review* **18** (2010) 279–315.

[79] J. Choquette, J. M. Cline and J. M. Cornell, *Early formation of supermassive black holes via dark matter self-interactions*, *JCAP* **07** (2019) 036 [1812.05088].

[80] S. Balberg, S. L. Shapiro and S. Inagaki, *Selfinteracting dark matter halos and the gravothermal catastrophe*, *Astrophys. J.* **568** (2002) 475 [astro-ph/0110561].

[81] A. Arvanitaki, M. Baryakhtar and X. Huang, *Discovering the QCD Axion with Black Holes and Gravitational Waves*, *Phys. Rev. D* **91** (2015) 084011 [1411.2263].

[82] H. Yoshino and H. Kodama, *The bosenova and axiverse*, *Class. Quant. Grav.* **32** (2015) 214001 [1505.00714].

[83] J. Kormendy and D. Richstone, *Inward bound: The Search for supermassive black holes in galactic nuclei*, *Ann. Rev. Astron. Astrophys.* **33** (1995) 581.

[84] J. Magorrian et al., *The Demography of massive dark objects in galaxy centers*, *Astron. J.* **115** (1998) 2285 [astro-ph/9708072].

[85] K. Heitmann, Z. Lukic, S. Habib and P. M. Ricker, *Capturing halos at high redshifts*, *Astrophys. J. Lett.* **642** (2006) L85 [astro-ph/0601233].

[86] Z. Lukic, K. Heitmann, S. Habib, S. Bashinsky and P. M. Ricker, *The Halo Mass Function: High Redshift Evolution and Universality*, *Astrophys. J.* **671** (2007) 1160 [astro-ph/0702360].

[87] S. Tacchella, S. Bose, C. Conroy, D. J. Eisenstein and B. D. Johnson, *A Redshift-independent Efficiency Model: Star Formation and Stellar Masses in Dark Matter Halos at $z \gtrsim 4$*, *Astrophys. J.* **868** (2018) 92 [1806.03299].

[88] T. Ishiyama et al., *The Uchuu Simulations: Data Release 1 and Dark Matter Halo Concentrations*, 2007.14720.

[89] S. Balberg and S. L. Shapiro, *Gravothermal collapse of selfinteracting dark matter halos and the origin of massive black holes*, *Phys. Rev. Lett.* **88** (2002) 101301 [astro-ph/0111176].

초록

정밀 우주론에 의해 ΛCDM 모델의 성공이 뒷받침되었지만, 허블상수의 우주배경복사 최적 피팅 값과 주변 우주에 존재하는 천체의 적색 편이 관측으로부터의 값 사이의 불일치가 존재한다. 이와 더불어 우주의 작은 규모 구조에서의 문제들과 약한 상호작용하는 무거운 입자 (WIMP) 암흑물질에 대한 실험적 증거의 부재로 인해 복잡한 구조를 가진 다양한 대체 암흑물질 모델들이 연구되어왔다. 이번 연구는 가벼운 스칼라 암흑물질에 대해 다룬다. 스칼라가 자연스럽게 작은 질량을 가지기 위해서 두 가지 가능성이 존재한다. 양-밀스 이론의 암흑 글루볼들은 점근적 자유도를 가진 게이지 섹터에서의 복합 입자로서 속박 에너지 정도의 질량을 가진다. 유사 골드스톤 보존은 가벼운 스칼라의 또 다른 가능성으로서, 게이지 섹터와 상호작용하는 암흑 액시온의 형태로 게이지 이론에 포함될 수 있다. 우주가 팽창함에 따라, 글루볼과 액시온의 에너지 밀도 등과 같은 배경 물리량들은 특별한 변화 과정을 가진다. 또한 글루온의 초기 온도 섭동이 글루온 온도에 의존하는 액시온의 잠재 에너지를 통해 액시온의 에너지 밀도 섭동을 유도할 수 있다. 마지막으로, 자체 상호작용하는 소수 암흑물질 구성요소로서 암흑 글루볼은 그들로 이루어진 은하 헤일로의 중력열붕괴를 통해 관측되고 있는 거대질량 블랙홀의 형성에 기여할 수 있다.

주요어: 암흑물질, 액시온, 글루볼, 자체 상호작용하는 암흑물질, 에너지 밀도 섭동, 거대질량 블랙홀, 중력열붕괴

학번: 2013-22985